

Modulating the Potency of BRD4 PROTACs at the Systems Level with Amine-Acid Coupling Reactions

Andrew McGrath, Haiyan Huang, Jean-Francois Brazeau, Zirong Zhang, Christopher O. Audu, Nadeem A. Vellore, Lu Zhu, Zhicai Shi, Jennifer D. Venable, Christine F. Gelin,* and Tim Cernak*



Cite This: <https://doi.org/10.1021/acs.jmedchem.4c02047>



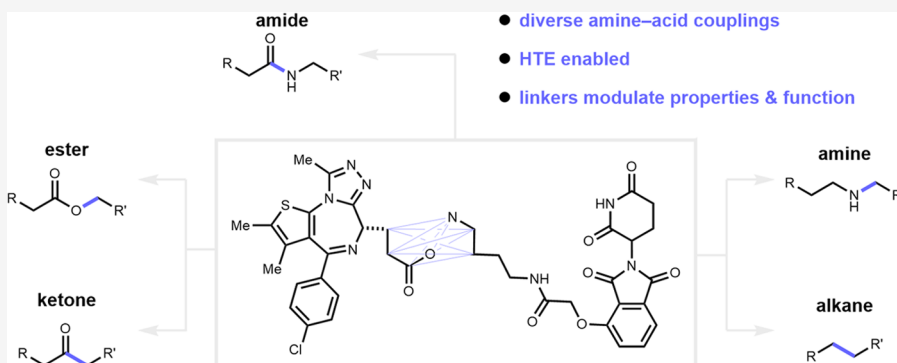
Read Online

ACCESS |

Metrics & More

Article Recommendations

Supporting Information



ABSTRACT: Protein degradation using proteolysis targeting chimeras (PROTACs) represents a promising therapeutic strategy. PROTACs are heterobifunctional molecules that consist of a target-binding moiety and an E3 ligase binding moiety, connected by a linker. These fragments are frequently united via amide bonds. While straightforward to synthesize, amides may impart suboptimal drug properties to the overall molecule. From a systems level perspective, we envisioned that the potency of PROTACs could be modulated through selection of reaction conditions—wherein different catalysts produce distinct linkers from the same two building blocks. We present a suite of BRD4 PROTAC degraders prepared via four new amine–acid coupling reactions alongside the classic amide coupling. Our findings reveal that variations in reaction conditions affect the physicochemical properties of PROTACs, resulting in a spectrum of properties. Notably, several new PROTACs demonstrated enhanced BRD4 degradation efficacy compared to those employing amide linkers, emphasizing the potential of systems chemistry as a therapeutic optimization strategy.

INTRODUCTION

Control over physicochemical properties using chemical synthesis is typically achieved by varying starting materials to introduce molecular diversity. Molecular functions such as selective tissue distribution or metabolic stability of pharmaceuticals are linked to physicochemical properties and chemical structure. While the connection of structure and function is well established, the use of reaction conditions to drive function, through a systems-level chemistry evaluation,¹ is underexplored. An interconnected and interdependent network of building blocks, reaction conditions, transformations, structures, properties, and function can be viewed on a systems level where, for instance, the choice of a reaction catalyst could drive a cellular phenotypic outcome (Figure 1a). For instance, Nelson, Warriner and Karageorgis reported an application of activity-directed diversity-oriented synthesis,² where diazoamides underwent diverse intramolecular rhodium-catalyzed cyclizations depending on the catalyst chosen, and yielded products with diverse bioactivities. We earlier demonstrated that intermolecular couplings of amines and acids could steer computed parameters such as physicochemical properties³ and

protein–ligand docking scores⁴ based on the selection of reaction conditions. Here, we experimentally validate control of compound bioactivity in an intermolecular setting through a systems level integration of interconnected parameters (Figure 1a). We envision that such systems chemistry explorations will become increasingly important since computational predictions of bioactivity are becoming more precise while synthesis and bioassay experiments becoming more automated.¹

The emergence of proteolysis targeting chimeras (PROTACs) as a powerful therapeutic modality exemplifies the significant impact of linker composition, not only on activity, but also on the bulk physicochemical properties of these protein degraders.^{5–10} PROTACs are heterobifunctional

Received: August 27, 2024

Revised: November 6, 2024

Accepted: November 21, 2024

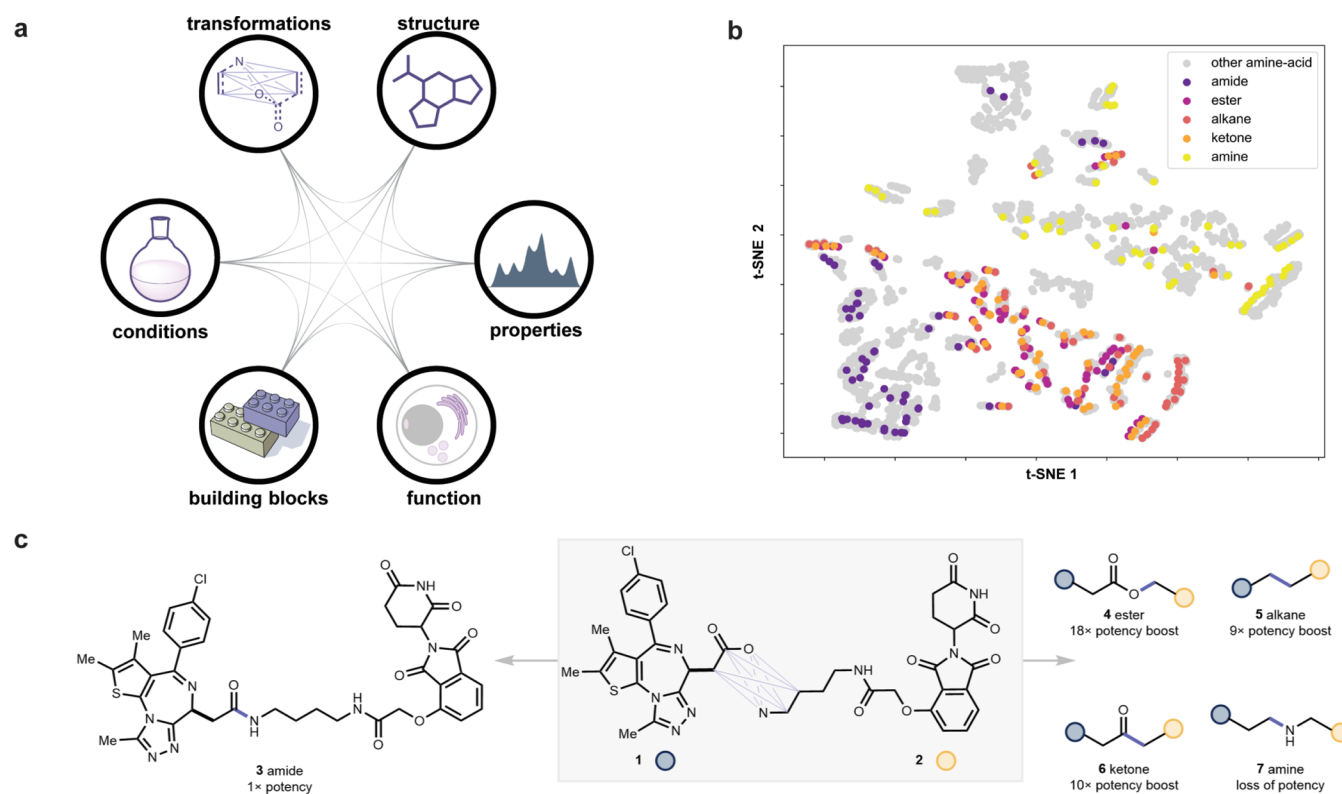


Figure 1. (a) Systems chemistry: building blocks, conditions, transformations, structure, properties, and function are interconnected and interdependent. (b) 80 transformations (ref 2) are applied to 1 and a collection of commercially available amine-containing partial PROTACs (see Supporting Information) to give a chemical space, displayed as a t-distributed stochastic neighbor embedding (tSNE), with amide, ester, amine, alkane, ketone products highlighted in color. (c) Diverse amine–acid couplings on 1 and 2 can produce amide (3), ester (4), alkane (5), ketone (6), or amine (7), congeners.

molecules that contain a ligand to recruit an E3 ubiquitin ligase, a ligand to bind the protein of interest (POI), and a linker conjoining the two ligands, leading to event driven pharmacology that is catalytic and agnostic of receptor occupancy.¹¹ As such, PROTACs have a unique ability to target “undruggable” proteins. The explosion of interest in PROTACs has led to an extensive, commercially available toolkit of linker and E3 ligase binding building blocks, most of which terminate in an amine or carboxylic acid. Indeed, the coupling amines and acids to form amides is one of the most popular methods in the synthesis of PROTACs.^{12,13} Other tactics include esterification,¹⁴ click chemistry,¹⁵ S_NAr,¹⁶ Buchwald–Hartwig coupling,¹⁷ and various other methods.^{18–20} In a conventional amide coupling, when a primary amine and carboxylic acid are united,²¹ the resultant amide motif bears one hydrogen bond donor (HBD) along with two hydrogen bond acceptors (HBA) and is neutral in charge. In this manner, the transformation itself can be viewed as leaving a physicochemical footprint on the product. However, if the conditions used in the reaction are modified and an ester is produced instead, the product has one less HBD. It follows that the properties, and thus the functional outcome, of a molecule is dependent not only upon the building blocks used to create it but also the transformation used to unite them. The diverse composition and arrangement of atoms accessed in this way allows for a fine-tuning of properties from two building blocks just by changing reaction conditions.⁴ When we applied 80 possible transformations³ on acid 1 and a suite of commercially available cereblon (CRBN) recruiting amines in silico, a diverse property space emerged (Figure 1b). The

properties of the molecules produced, including molecular weight, LogP, formal charge, and polar surface area (PSA) (see Supporting Information) were calculated and compared using a t-distributed stochastic neighbor embedding (tSNE) (Figure 1b). This analysis revealed the transformations forming amide (purple dots) and amine products (yellow dots) in general occupy their own chemical space, suggesting these transformations impart a larger effect on the overall properties of the molecule. Comparatively, the ester (pink dots), alkane (red dots), and ketone products (orange dots) overlap, indicating these transformations exert a more nuanced effect on the property space occupied by the products. This is further exemplified by the incorporation of basic amines into the linker portion of the starting amine (c.f. orange dots in the space mostly occupied by yellow dots). Notable pockets of this space remain inaccessible (gray dots), for instance from transformations that retain the carboxylic acid or incorporate bond rearrangements (see Supporting Information), representing synthetic methods that merit future investigation. However, the five transformations demonstrated here indeed cover a breadth of space and structure activity relationships when starting from the same two building blocks.

Herein, we developed a suite of amine–acid PROTACs linking reactions that produced either an amide, ester, amine, alkane, or ketone linkage using the well-studied bromodomain inhibitor JQ1 1 and cereblon (CRBN) binding pomalidomide-derived amine 2 to yield the classic PROTAC dBET1 (3) and derivatives 4–7 of (Figure 1c).²² Each of these methods provides a unique way to pair a POI and a partial PROTAC, and the resultant compounds span a range of physicochemical

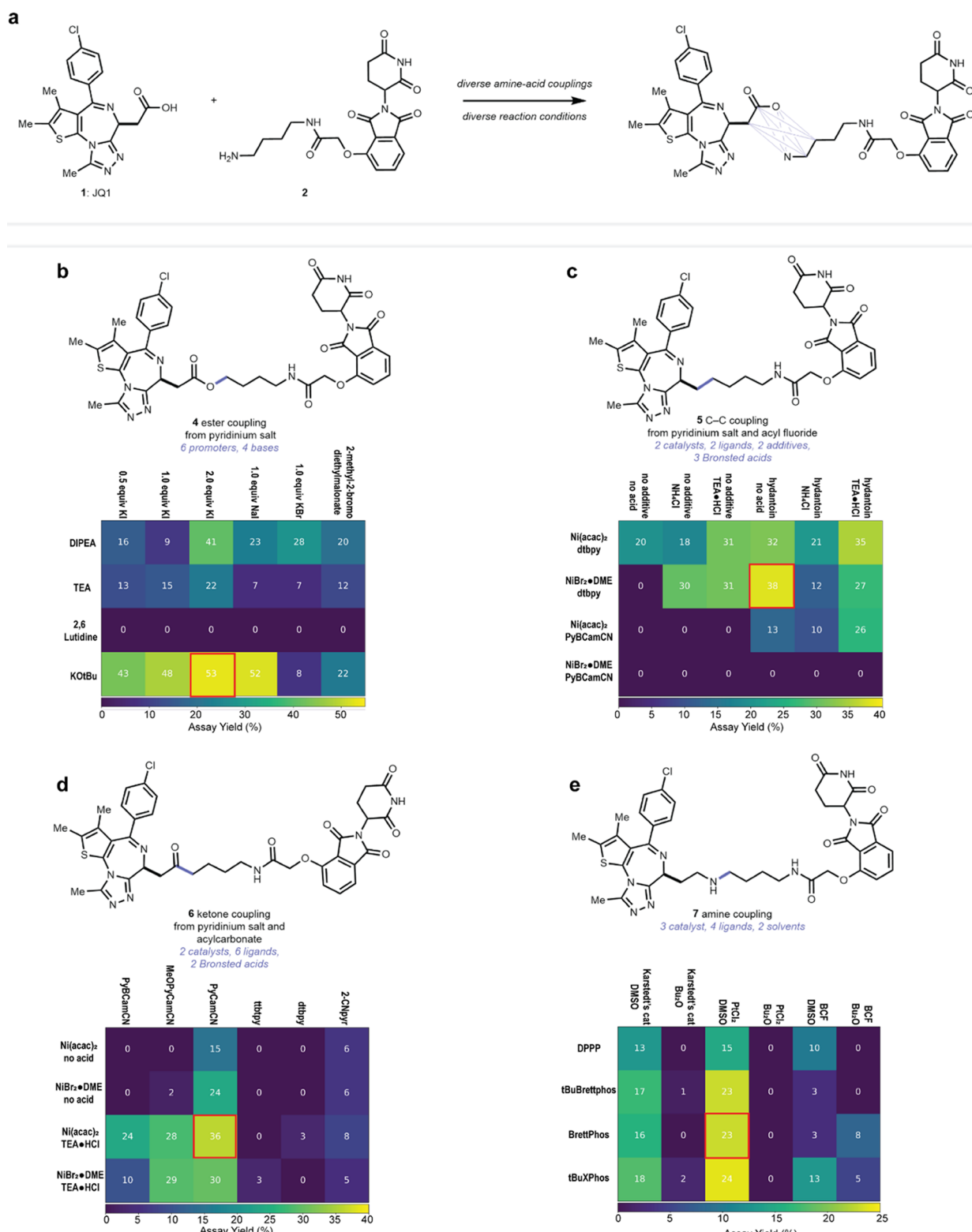


Figure 2. (a) Developing diverse reaction conditions to produce ester, amine, alkane, and ketone-linked analogs of amide dBET1 (3) using high-throughput experimentation. Assay yields were determined by UPLC-MS. (b) Ester array conditions: 10 μmol of 1 (1.0 equiv), 10 (1.0 equiv), base (1.0 equiv) and additive (equiv listed) per well. (c) Alkane array conditions: 5 μmol (2.0 equiv) of 8, 10 (1.0 equiv), nickel catalyst (40 mol %), ligand (40 mol %), imide additive (2.0 equiv), Brønsted acid (2.0 equiv), and manganese (4.0 equiv) per well. (d) Ketone array conditions: 5 μmol (2.0 equiv) of 9, 1.0 equiv of 10, nickel catalyst (40 mol %), ligand (40 mol %), additive (2.0 equiv), and manganese (4.0 equiv) per well. (e) Amine array conditions: 15 μmol of 1 (1.5 equiv), 2 (1.0 equiv), catalysts (5 mol %), ligand (10 mol %), and phenylsilane (4 equiv) per well. All wells contain 100 μL of solvent. PyBCamCN = (2Z,6Z)-N'2,N'6-Dicyanopyridine-2,6-bis(carboximidamide), MeOPyCamCN = 4-methoxy-N-cyanopicolinimidamide PyCamCN = N-cyanopicolinimidamide, ttbipy = 4,4',4"-tritert-Butyl-2,2':6',2"-terpyridine, dtbpy = 4,4-ditert-butylbipyridine, 2CNPyr = 2-cyanopyridine, Karstedt's cat = Platinum(0)-1,3-divinyl-1,1,3,3-tetramethyldisiloxane complex.

and pharmacological properties. Our suite of heterobifunctional degraders, accessed from these CCRN amines and carboxylic acid coupling transformations was also applied to a von Hippel–Lindau (VHL) targeting amine. The results of this systems-level study highlight the intricate connectivity between reaction conditions, transformations, and biological function.

RESULTS AND DISCUSSION

Optimization of Reaction Conditions. Our studies initiated with a campaign to identify diverse reaction conditions for linking **1** and **2** that would produce PROTAC molecules **3–7**. We used miniaturized high throughput experimentation (HTE), which has emerged as a powerful tool in the navigation of reaction space.^{23–26} In addition to allowing a rapid assessment of the interplay of multiple reaction variables, the use of miniature glass vials allows for conservation of precious starting materials,²⁷ such as complex partial PROTAC building blocks. HTE investigation of the four targeted amine–acid coupling transformations esterification, alkylation, ketonylation, or amination was conducted surveying 24 unique reaction conditions each. Reactions were performed on less than 10 μmol scale of starting material **2** per well (Figure 2a). Automatable amine–acid esterification reactions have been developed by our lab for both alkyl²⁸ and aryl amines.²⁹ In the alkyl amine setting, the esterification proceeds via activation of the alkyl amine as its triphenylpyridinium salt³⁰ and aging with a carboxylic acid in the presence of *N,N*-diisopropylethylamine (DIPEA) and potassium iodide (KI). When **1** and the pyridinium salt of **2** were subjected to these conditions, the desired ester was observed alongside an undesired isobaric compound presumed to be from imine N-alkylation (Supporting Information, Figure S10). Thus, a 24-well reaction array examining different promoter additives and bases was performed to identify alternative reaction conditions for the formation of desired ester **4** (Figure 2b). In general, stronger bases facilitated the formation of the desired ester product. For instance, potassium *tert*-butoxide yielded **4** as the exclusive product whereas lutidine exclusively formed the undesired adduct. DIPEA and triethylamine (TEA) gave mixtures of both the desired product and the undesired adduct. Potassium bromide (KBr) and bromomethyldiethyl malonate facilitated the reaction as additives, but in lower yield than KI or sodium iodide (NaI). The best performing conditions used KI and potassium *tert*-butoxide and gave **4** in 53% assay yield and 54% isolated yield. This protocol complements recently reported methods to access ester-linked PROTACs via total synthesis.¹⁴

To access alkane and ketone linked products, we explored nickel-catalyzed reductive cross-coupling conditions. Related methods employing nickel as the metal catalyst have emerged as a powerful tool to link pyridinium salts^{31–35} and activated carboxylic acids,^{36–39} and we hypothesized that a related nickel-catalyzed system would best facilitate the formation of alkane (**5**) and ketone (**6**) targets. We began our investigation through coupling acyl fluoride **8** (Figure 3), generated *in situ* from **1** using tetramethylfluoroformamidinium hexafluorophosphate (TFFH) and proton sponge, and **10** (the pyridinium salt of **2**). Subjecting these coupling partners to nickel(II) bromide-glyme ($\text{NiBr}_2\text{-DME}$), 4,4-di-*tert*-butylbipyridine (dtbpy), and elemental manganese produced alkane product **5**. A thorough investigation of the interplay of imide additives (see Supporting Information),⁴⁰ nickel sources, ligands, and Brønsted acid additives (Figure 2c) was conducted. We found

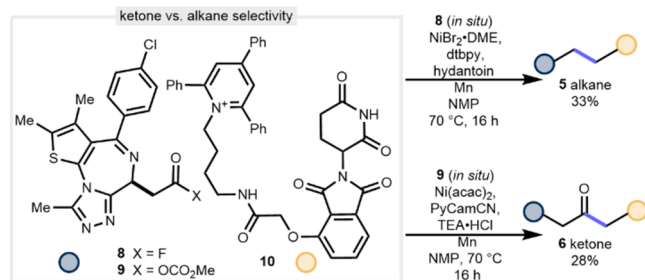


Figure 3. Change in ligand switches the selectivity for the synthesized product from alkane **5** to ketone **6**. Reactions conducted using **8** or **9** (2.0 equiv), **10** (1.0 equiv), nickel catalyst and ligand (40 mol % each), additive (2.0 equiv), and manganese (4.0 equiv) at 0.025 M.

that hydantoin increased alkane formation whereas the inclusion of Brønsted acids was detrimental. $\text{NiBr}_2\text{-DME}$, and dtbpy were observed to be the optimal catalyst and ligand combination giving **5** in 38% assay yield, which translated to a 33% isolated yield on scale up.

In our investigation of ligands to synthesize alkane **5**, we observed that ligand choice influenced the distribution of mixtures of **5** and ketone **6** (see Supporting Information). Based on these observations we hypothesized we could access **6** through careful selection of catalyst, ligand and additive. Thorough investigation revealed the need to explore other activation strategies (see Supporting Information). For substrates derived from **1**, we determined acyl carbonates³⁸ to be a viable activating group. Subsequently, JQ1 (**1**) was activated *in situ* by using dimethylidicarbonate (DMDC). After determining our optimal activating group, we investigated the use of imides, Bronsted acids, and ligands (Figure 2d). We found the ligand (*Z*)-*N*-cyanopicolinimidamide (PyCamCN) maximized the yield of **6**, whereas dtbpy gave alkane **5** exclusively. Notably, in contrast to our findings in the C–C coupling of **1** and **2**, the use of imide additives hindered ketone formation while triethylammonium hydrochloride ($\text{NEt}_3\text{-HCl}$) was found to increase the yield. We selected *in situ* activation of **1** with DMDC and catalyzed ketonylation with nickel(II) acetylacetone $\text{Ni}(\text{acac})_2$, PyCamCN, and $\text{NEt}_3\text{-HCl}$ as optimal conditions to deliver **6** in 36% assay yield (28% isolated yield). We were intrigued by the rapid decarbonylation of the acyl fluoride **8** to give alkane product **5** as opposed to ketone product **6** when subjected to nickel and dtbpy, in contrast to literature reports (Figure 3).^{7,36} Mechanistic investigations in our lab and others^{37,41–43} have highlighted that subtle effects govern the decarbonylation event in nickel-catalyzed reductive cross-couplings. In addition, ligands may also play a role in governing the kinetics of decarbonylation; when the acyl carbonate of **1** and pyridinium salt of **2** were subjected to $\text{NiBr}_2\text{-DME}$ and dtbpy, only the decarbonylated alkyl coupling product **5** was observed, albeit in lower yield. To further probe this effect, we investigated other amine and carboxylic acid coupling partners under our reaction conditions (see Supporting Information). In general, we have discovered that selectivity for C–C coupling is consistent in the case of primary pyridinium salts whereas only the ketone product is observed when using secondary pyridinium salts. The rapid decarbonylation is also observed in carboxylic acids containing a β -diphenyl imine group. Further investigations into this effect are ongoing in our lab.

We next turned our attention to the formal reductive amination between **1** and **2** to arrive at amine-linked products

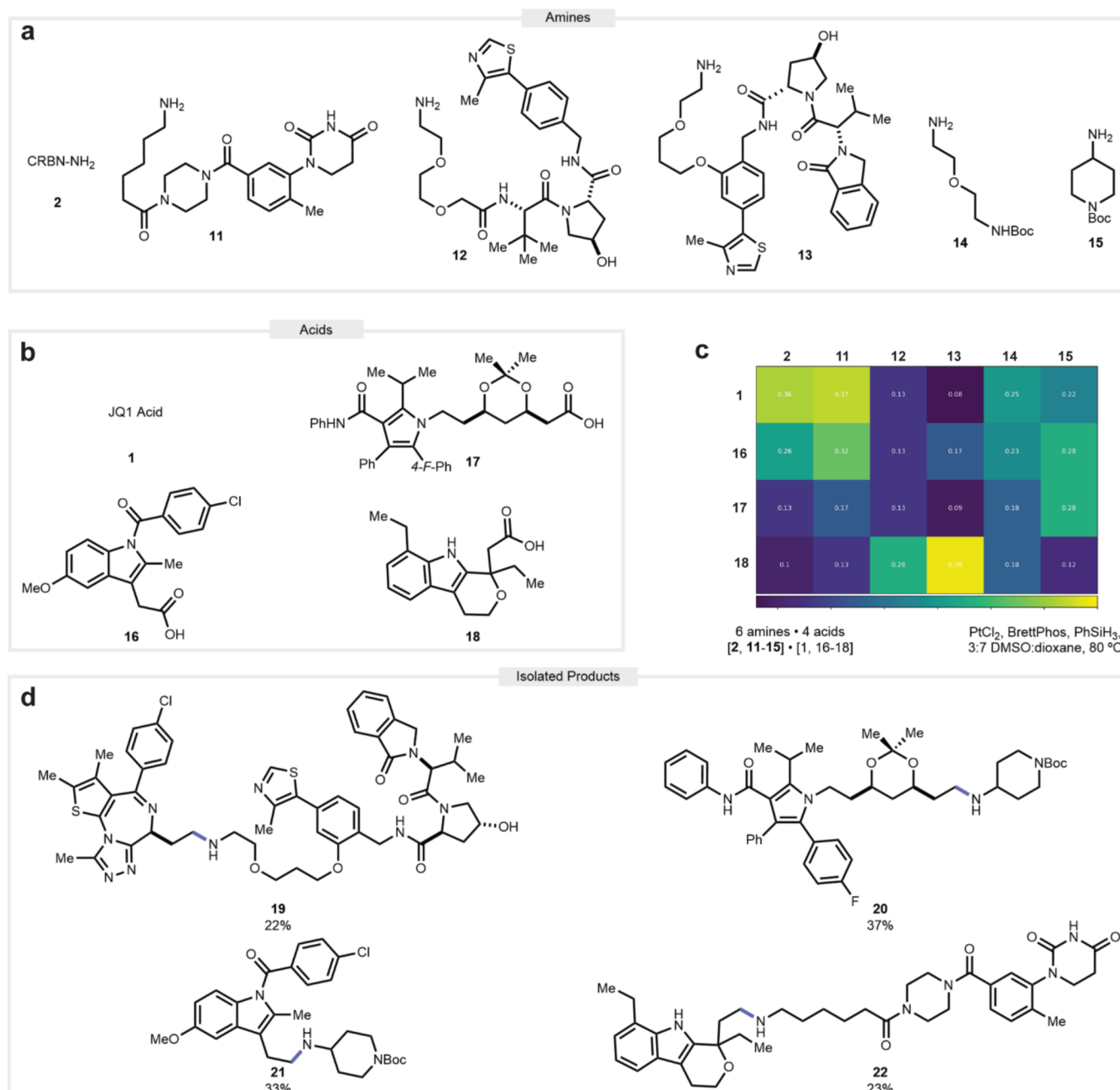


Figure 4. Reductive amination conditions applied to a library of (a) 6 amines and (b) 4 acids. All reactions conducted using 10 μmol of amine (1.0 equiv) and 15 μmol of acid (1.5 equiv), PtCl₂ (5 mol %), BrettPhos (10 mol %) and PhSiH₃ (5.0 equiv) at 0.1 M. (c) Results of the screen (d) Isolated yields upon scale up of select compounds on 0.100 mmol scale relative to the amine starting material.

directly from an amine and acid. Based upon literature precedent,^{44,45} we believed the desired reactivity could be achieved using either platinum catalysts or *tris*(pentafluorophenyl)borane (BCF). BCF in dibutylether (Bu₂O) produced a trace amount of desired amine 7 along with amide 3 and recovered starting material, and no reduction of the amide bond or the four other carbonyls. Further investigation of solvent effect demonstrated that DMSO outperforms other polar aprotic solvents (see *Supporting Information*) suggesting that performance is not entirely driven by solubility. Based upon these data we planned a screen investigating solvents, catalysts, and ligands. Three catalysts (two based on platinum along with BCF), and four phosphine ligands, were surveyed by HTE using DMSO or dibutyl ether

as solvent. Our observations confirmed that DMSO is essential to achieving reactivity with these complex substrates, which contrasts reports on simpler substrates.^{44–46} Additionally, platinum catalysis outperformed boron catalysts with platinum(II) chloride being an optimal catalyst and BrettPhos as a preferred ligand.

Exploration of Substrate Scope and Reaction Scale-Ups. To further explore the scope of the reductive amination reaction we applied our optimized condition to an array of six amines including four partial PROTACs (2, 11–13), two linker type molecules (14, 15) (Figure 4a) and four pharmaceutically relevant carboxylic acids (1, 16–18) (Figure 4b). Since we have seen that CRBN targeting ligands such as 2 and 11 generally perform better in pure DMSO, and other

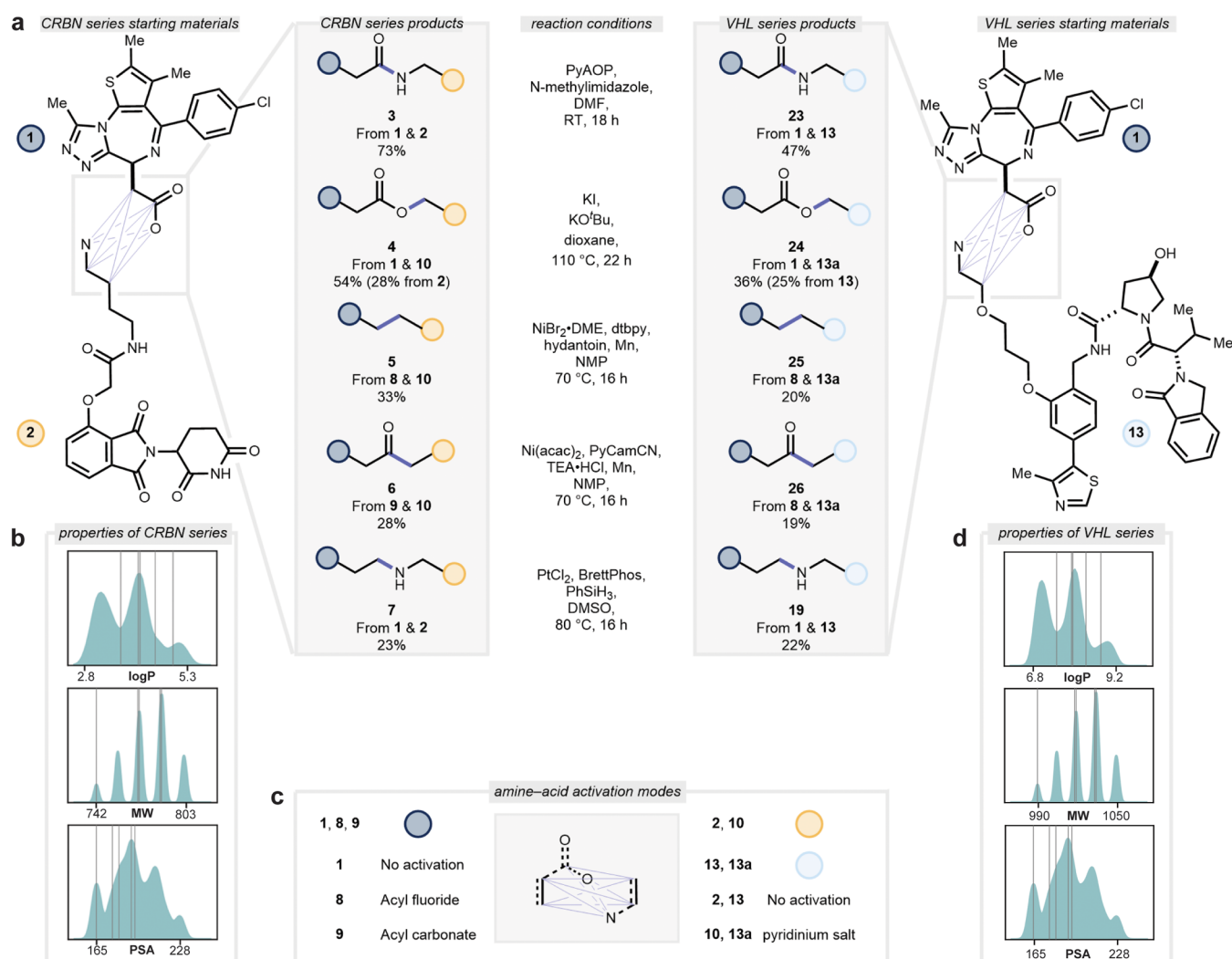


Figure 5. (a) Five transformations applied to **1** and **2** (CRBN), as well as **1** and **13** (VHL). All reactions conducted at 0.100 mmol scale relative to the amine. Amide conditions: **1** and **2** (1.0 equiv), PyAOP (1.0 equiv), and *N*-methyldimidazole (1.0 equiv) in 1.0 mL of solvent (0.1 M). Ester reaction conditions: **1** and **10** (1.0 equiv), KI (2.0 equiv), and KO*t*Bu (1.0 equiv) in 1.0 mL solvent (0.1 M). CC and Ketone conditions: **1** (2.0 equiv), **2** (1.0 equiv), nickel catalyst (40 mol %), ligand (40 mol %), additive (2.0 equiv), and manganese (4.0 equiv) in 2.0 mL solvent 0.05 M. Amine conditions: **1** (1.5 equiv) and **2** (1.0 equiv), PtCl₂ (5 mol %), BrettPhos (10 mol %), and PhSiH₃ (5.0 equiv). (b) Chemoinformatic analysis of **3–7**. (c) Methods used to activate the amine or acid coupling partner. (d) Chemoinformatic analysis of **19, 23–26**.

systems perform better using a mixture of DMSO and dioxane, we settled on 30% DMSO in dioxane. These conditions appear broadly applicable to late-stage derivatization as we saw product formed in every well (Figure 4c). This is remarkable as the reactions are performed in the presence of functionalities such as alcohols (12,13), acetonides (17), a dihydrouracil (11), and an indole (16). Additionally, the reaction works on aliphatic as well as benzylic acids. To validate our screening protocol we isolated products from four wells on a 0.1 mmol scale (19–22) (Figure 4d). In each of these reactions, we did not observe reduction of other carbonyls present in the molecule. These results as well as control experiments where the amine was omitted (see Supporting Information) suggest a pathway where an aldehyde intermediate is formed prior to coupling as opposed to amide formation and subsequent reduction.^{44,45,47} The ester, alkane, and ketone transformations as well as the amide coupling were also applied to the same library of amine-acid coupling partners (see Supporting Information).

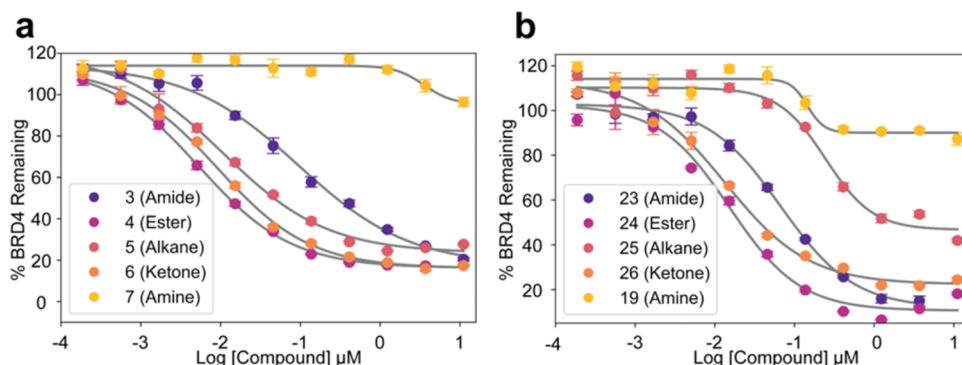
With optimized conditions for each transformation, we turned our attention toward the isolation of each compound on synthetically useful scale (0.1 mmol) (**Figure 5a**) using VHL targeting amine **13**.^{7,8,48}

We observed similar reactivity trends despite the incorporation of potentially sensitive functional groups. Isolated yields on preparative scale found to correlate well with assay yield for each transformation and delivered both the CRBN and VHL based PROTACs in acceptable quantity. Our amide conditions (see [Supporting Information](#)) yielded compound **3** in 73% and compound **23** in 47% yield, respectively. Applying our esterification conditions to each substrate yielded ester **4** in 54% and ester **24** in 36% yield. Further, a one-pot protocol (see [Supporting Information](#)) was developed to give **4** directly from **1** to **2** in 28% yield. A slightly modified protocol using two equivalents of base was applied to the hydrochloride salt of **13** to give **24** in 25% yield. Applying our alkane-forming conditions yielded **5** in 33% and **25** in 20% yield, respectively. Application of our ketone-forming conditions yielded **6** and **26** in 28% and 19% yield, respectively. Finally, our conditions for

Table 1. Experimental Physicochemical Properties and BRD4 HTRF Degradation Values^a

E3 ligase	linker type (#)	MW	CHI Log $D_{7.4}$	BRD4 HTRF degradation DC ₅₀ (nM)	BRD4 HTRF degradation D_{max} (%)
CRBN	amide (3)	785	2.16	95.0 ± 7.2	80
CRBN	ester (4)	786	2.68	5.4 ± 1.0	83
CRBN	alkane (5)	742	2.81	10.8 ± 0.9	76
CRBN	ketone (6)	770	2.57	9.2 ± 1.0	85
CRBN	amine (7)	771	1.66	>11 000	2
VHL	amide (23)	1033	2.78	68.3 ± 6	87
VHL	ester (24)	1034	3.25	15.8 ± 1.5	89
VHL	alkane (25)	990	3.38	228.0 ± 16.7	58
VHL	ketone (26)	1017	3.16	13.4 ± 0.9	79
VHL	amine (19)	1018	2.30	>11 000	14

^aNote: Values reported are the mean ± SEM of a single experiment run in quadruplicate.

**Figure 6.** BRD4 HTRF degradation assay: (a) CRBN series degradation curves (3–7). (b) VHL series degradation curves (19, 23–26).**Table 2.** Target Engagement for CRBN Analogs (3–7)^a

linker type (#)	BRD4-BD1 HTRF (nM)	nanoBRET live (nM)	nanoBRET permeabilized (nM)	nanoBRET RBA
amide (3)	16.0 ± 1.1	528.5 ± 35.0	86.3 ± 4.8	6.1
ester (4)	2.3 ± 0.1	263.7 ± 7.6	68.8 ± 4.4	2.4
alkane (5)	66.9 ± 1.1	503.5 ± 19.9	120.7 ± 14.2	4.2
ketone (6)	24.2 ± 0.9	421.8 ± 21.1	107.1 ± 15.9	3.9
amine (7)	453.2 ± 18.4	11272 ± 1992.7	102.0 ± 4.9	110.5

^aEngagement assessed by BRD4-BD1 HTRF displacement assay and cellular nanoBRET CRBN-tracer assay in live and permeabilized conditions. Values reported are the mean ± SEM of a single experiment run in triplicate for the BRD4-BD1 HTRF assay, and five technical replicates for the CRBN cellular nanoBRET assay.

reductive amination afforded **7** in 23% yield. It was found necessary to use 10% DMSO in dioxane as solvent to achieve optimal reactivity for the synthesis of **19**. This adjustment furnished **19** in 23% yield. It is noteworthy that we did not observe opening of the glutarimide ring under any of our reaction conditions.^{49,50}

Properties of Isolated PROTACs. With nine new dBET1 analogs in hand, cheminformatic calculations were performed on each molecule to demonstrate that we can effectively modulate the properties of each final PROTAC by changes to the linker composition (Figure 5b,d). While bulk properties are influenced by choice of building blocks (**2** versus **13**), each transformation also imparts its own effect on the overall properties of the molecule, which is a key tenet of our systems chemistry vision. Notably, removal of one HBD (amide/amine versus ester/alkane/ketone) can shift the calculated log P by over one log unit relative to the amide (**3**) as well as having a significant impact on polar surface area (PSA) (see Supporting Information). This was validated experimentally through determination of chromatographic hydrophobicity index (CHI) log $D_{7.4}$. For amide **3**, the experimental value was

determined to be 2.16, with ester **4**, alkane **5**, and ketone **6** giving values of 2.68, 2.81, and 2.57 respectively (Table 1). Meanwhile, protonatable amine **7** had a significantly lower log $D_{7.4}$ at 1.66. The same trend follows for the VHL series with amide **23** having log $D_{7.4}$ of 2.78 compared to 3.25, 3.38, 3.16, and 2.30 for **24**, **25**, **26**, and **19**. The ability to modulate log $D_{7.4}$ coupled with the option to vary molecular weight by up to 44 g/mol highlights the impact that reaction conditions can have on function when optimizing degraders.⁵¹

In Vitro Activity of BRD4 PROTACs. Having established conditions to scale up and isolate the 10 BRD4 PROTACs (**3–7**, **19**, **23–26**), in vitro profiling to assess BRD4 degradation was initiated. We tested both CRBN-based (**3–7**) as well as VHL-based (**19**, **23–26**) PROTACs in HEK293 cells to readout endogenous BRD4 degradation DC₅₀ and D_{max} values,⁵² using a BRD4 homogeneous time-resolved fluorescence (HTRF) degradation assay (Figure 6). In addition, to distinguish on target BRD4 degradation from general cell toxicity, CellTiter-Glo (CTG) was also conducted (see Supporting Information). Within the CRBN-BRD4 PROTAC series, we observed several molecules with more efficient

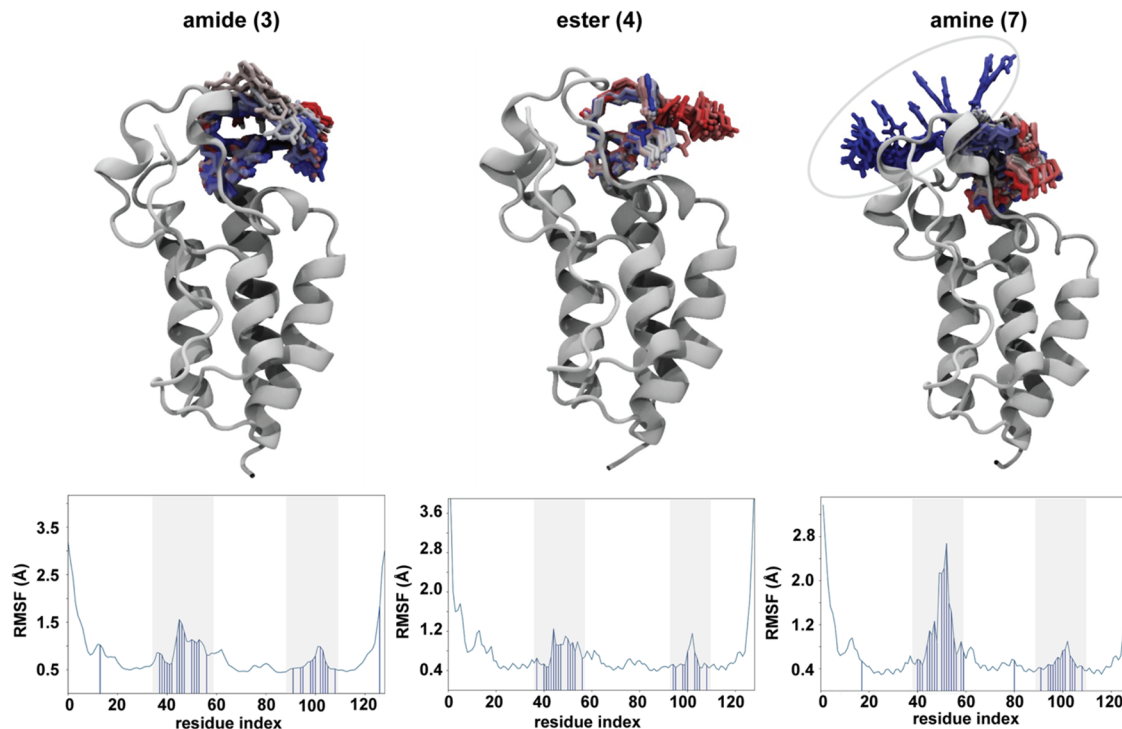


Figure 7. Molecular dynamic simulations of PROTACs 3, 4, and 7 bound to the BRD4-BD1 crystal structure (PDB: 6BOY).⁵⁵ Time-lapse snapshots from 250 ns simulations are shown overlaid and depicted using color changes from red to blue indicating initial to final binding pose. The region highlighted with a gray circle for the complex with 7 demonstrates that the amine congener samples many different conformations over the 250 ns simulation, which is observable also in the RMSF plot below, suggesting that the complex with 7 is less stable and hence supporting the observation of lower affinity. RMSF = root-mean-square fluctuation.

BRD4 degradation than amide dBET1 (3) (Figure 6a, Table 1). The ester 4, alkane 5 and ketone 6 were more potent than amide 3, with DC₅₀ values of 5.4, 10.8, 9.2, and 95.0 nM, respectively (Table 1). BRD4 degradation comparable to amide 3 (D_{\max} 80%), was observed for 4, 5, and 6 (83%, 76%, and 85% at 24 h). In comparison, the amine analog 7 was not successful at degrading BRD4 with a DC₅₀ of >11 μ M. In general, the VHL-based PROTACs 19, 23–26, follow the same trend in BRD4 degradation (see Figure 6b), albeit DC₅₀ values are higher and D_{\max} values lower. Ester 24 and ketone 26 are the most efficient degraders of BRD4 in the VHL series, with DC₅₀ values of 15.8 and 13.4 nM (D_{\max} values of 89% and 79%, respectively) (Table 1). VHL-derived alkane 25 has ~20-fold higher DC₅₀ and diminished D_{\max} value relative to CRBN-derived alkane 5, likely due to the reduced binding to BRD4 and VHL proteins (see Table S20 in Supporting Information).

To understand the observed BRD4 degradation results that arose from changing the linker, we measured target engagement of the heterobifunctional degraders to BRD4 protein and the corresponding E3 ligase (Table 2). Binding affinity of the PROTACs to BRD4 3–7 was assessed in a BRD4-BD1 biochemical probe displacement assay to bromodomain BD1. E3 ligase engagement was evaluated in a cellular CRBN or VHL nanoluciferase-based bioluminescence resonance energy transfer (nanoBRET) assay dependent on the PROTAC synthesized. The cellular nanoBRET target engagement assay was used as a surrogate to examine PROTAC cellular permeability.⁵³ The assay was performed in both live and permeabilized (lytic) cells and intracellular availability was determined by calculating the relative binding affinity (RBA).⁵⁴

Table 2 shows the data for the five CRBN-BRD4 PROTACs using amide 3 as a benchmark, which has a BRD4 affinity of

16.0 nM, and CRBN binding of 528.5 nM (live cells) and 86.3 nM (permeabilized cells). Of the newly synthesized analogs, ester 4, alkane 5, and ketone 6 maintain binding with IC₅₀ values of 2.3, 66.9, and 24.2 nM for BRD4, respectively. Notably, removal of the carbonyl moiety in alkane 5 does not result in a significant loss in BRD4 affinity (Table 2). Looking at the RBA values, a decrease is seen for ester 4, alkane 5, and ketone 6, (RBA: 2.4, 4.2, and 3.9, respectively, relative to 3). This is possibly because these three analogs have higher measured CHI Log D_{7.4} correlating with an anticipated increase in permeability. All three of these analogs have the N–H group removed, so have one fewer HBD than amide 3. The SAR trend observed for BRD4 degradation has 4–6 as the most potent degraders and the improvement in permeability and BRD4 affinity could potentially explain the observed degradation. VHL degraders 19, 23–26 occupy less drug-like space due to their higher molecular weight and larger number of HBD but still show the same rank order in BRD4 target engagement and improved RBA values (see Supporting Information). However, the lower VHL affinity in live cell nanoBRET for 19, 23–26 may explain the rightward shift in DC₅₀ values (Table 1). High degradation efficacy of BRD4 is retained by VHL PROTACs with D_{\max} ranging from 58% to 83%. Amine 7 shows a greater than 100-fold difference in IC₅₀ between the live and permeabilized cells and this can be attributed to the basic amine in the linker hampering permeability into cells. Additionally, the BRD4 potency of amine 7 is 453 nM compared to 16 nM for amide 3. Further investigation of this significant shift in potency to the protein of interest was investigated computationally.

Molecular Dynamics Simulations to Elucidate Differences in Binding and Degradation. To understand the

differences in binding affinity of potent versus binders with poor affinity, molecular dynamic (MD) simulations of BRD4-BD1 in the presence of amide 3, ester 4, and amine 7 were conducted in explicit solvent conditions. Sampled conformations from the 250 ns MD simulations are shown in Figure 7 (initial pose is shown in red and final pose in blue). Based on the simulations, both amide 3 and ester 4 maintain key interactions with the BRD4 binding site. In contrast, amine 7, due to the presence of a charged linker, interacts with Asp144 and engages in an intramolecular hydrogen bond with the imine nitrogen of the azepine on the POI motif during the course of the simulation (see Supporting Information for 2D interaction diagram). These observed interactions significantly alter the conformation of amine 7 as seen during MD simulation (Figure 7). Furthermore, the BRD4-BD1 protein complex displays significantly higher root-mean-square fluctuation (RMSF) near the binding region of the amine in 7 compared to the same region for amide 3 or ester 4. This instability of 7 interaction with BRD4 along with its conformational preferences could influence productive ternary complex formation and contribute to the negligible degradation performance we observed for this amine-linked derivative.

Investigation of Ternary Complex Formation. To explore how changing the PROTAC linkers influenced the formation of a productive ternary complex, we evaluated PROTAC induced ternary complex formation between CRBN/DDB1 and BRD4-BD1 in vitro, using an HTRF assay (Figure 8a). When titrating the PROTAC compounds,

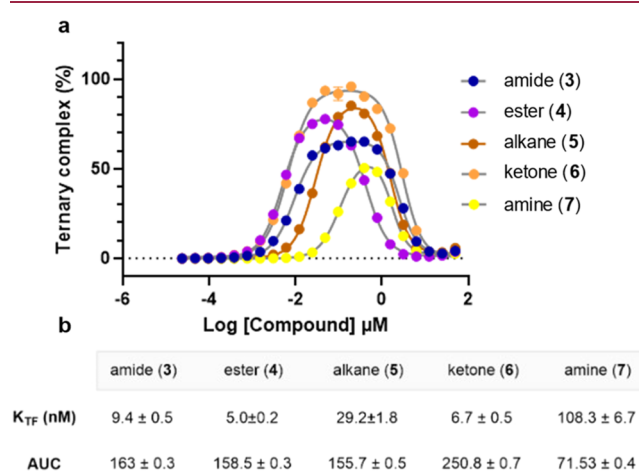


Figure 8. Experimental PROTACs-driven ternary complex formation in vitro. (a) Ternary complex formation of CRBN/DDB1:PROTAC::BRD4-BD1 assessed for PROTACs 3–7 by HTRF assay. Ternary complex (%) is calculated by HTRF signal of each PROTAC against the HTRF peak signal when treated with dBET6 (98 nM) (see Supporting Information for structure of dBET6). Values reported are the mean ± SEM of a single experiment in duplicate for the CRBN-BRD4 ternary complex assay. (b) Assay metrics of ternary complex formation concentration K_{TF} and AUC for the ternary complex formation by PROTACs 3–7.

we observed “bell-shaped” dose response curves, typical of a hook effect, at high concentrations of PROTACs due to increasing competition from binary complexes. The area under the bell-shaped curve (AUC) quantifies the amount of ternary complex formed and correlates with its stability. The ternary complex peak formation AC₅₀ values (K_{TF}) for compounds (3–7) correlate well with BRD4 degradation DC₅₀ (Figure

8b). Notably, amine 7 exhibits the weakest ternary complex formation compared to other PROTACs, observed as the lowest AUC (71.53) and a right-shifted dose response for ternary complex formation ($K_{TF} = 108$ nM), possibly due to its weaker binding affinity to BRD4 and CRBN. This is consistent with the molecular dynamic simulation (Figure 7) that the charged linker for amine 7 is disfavored for stable ternary complex formation and the observed PROTAC rank order for BRD4 degradation (Table 1).

CONCLUSIONS

In conclusion, a systems chemistry approach was used to link reaction conditions to PROTACs functions. By harnessing the power of HTE we have developed four unique amine–acid transformations, esterification, alkylation, ketonylation, and amination that proceed via intermediates that are generated in situ or prepared in a single step with no need for chromatography. Using these methods we quickly accessed a suite of BRD4 degraders with modifications to the linker from the same amine and acid-derived building blocks. Importantly these adjustments to the linker connectivity have been achieved using JQ1 as the target binding moiety and two workhorse E3 ligase recruiters (CRBN and VHL). The ester, ketone, and alkane transformations do not have the HBD moiety that is present in the amide analog, leading to higher log D values, increased cellular permeability, and lower RBA values in the E3 cell target engagement assay. The structural changes also affect binding to the target protein of interest, with removal of the carbonyl having the largest effect. These combined effects led to more potent degraders when the amide is exchanged for an ester, alkane, or ketone, but ineffective BRD4 degraders were observed with an amine linker. Experimental and computational studies indicate that amine 7 shows weaker target engagement, ternary complex formation, and BRD4 degradation. New amine-acid coupling reactions clearly impact the properties of PROTACs. These new reactions enable the creation of matched pairs of degraders with varied function. Taken together our results suggest a systems chemistry approach can have a profound impact on the biological activity of a molecule simply by modifying reaction conditions when coupling the same two building blocks.

EXPERIMENTAL SECTION

Chemistry General. All reactions were conducted in oven- or flame-dried glassware under an atmosphere of nitrogen unless stated otherwise. Reactions were set up in an MBraun LABmaster Pro Glove Box (H_2O level < 0.1 ppm, O_2 level < 0.1 ppm), or using standard Schlenk technique with a glass vacuum manifold connected to an inlet of dry nitrogen gas. N-methylpyrrolidinone was purchased as anhydrous and degassed by sparging overnight with nitrogen. Other solvents were purchased as anhydrous and used as received. Reagents were purchased from Sigma-Aldrich, Alfa Aesar, Oakwood Chemical, Ambeed, or TCI Chemical. All chemicals were used as received. Glass 1-dram (Fisherbrand parts No. 03-339-21B) or 2-dram vials (Fisherbrand parts No. 03-339-21D or ChemGlass #CG-4912-02) were used as reaction vessels, fitted with standard screwcaps (#03-452-225 or #03-452-300) or with Teflon-coated silicone septa (#CG-4910-02 or CG-4910-02), and magnetic stir bars (Fisher Scientific #14-513-93 or #14-513-65; stirbars.com #SBM-0803-MIC or #SBM-1003-MIC).

¹H NMR spectra were recorded on a Varian MR-500 MHz, Varian MR-400 MHz, Bruker DPX, DRX, or AV spectrometers. Chemical shifts are reported in parts per million (ppm) and the spectra are calibrated to the resonance resulting from incomplete deuteration of

the solvent (CDCl_3 : 7.26 ppm; $\text{DMSO}-d_6$: 2.50 ppm, qn; $\text{MeOD}-d_4$: 3.31 ppm, qn; Acetonitrile- d_3 : 1.94 ppm, qn). ^{13}C NMR spectra were recorded on the same spectrometers with complete proton decoupling. Chemical shifts are reported in ppm with the solvent resonance as the internal standard (CDCl_3 : 77.16 ppm, t; $\text{DMSO}-d_6$: 39.52 ppm, sept; $\text{MeOD}-d_4$: 49.00 ppm, sept, Acetonitrile- d_3 : 1.39 ppm, m, 128.39 ppm, s.). Data are reported using the abbreviations: app = apparent, s = singlet, d = doublet, t = triplet, q = quartet, p = pentet, h = hextet, m = multiplet, comp = complex, br = broad. Coupling constant(s) are reported in Hz. ^{19}F NMR spectra were recorded on the same spectrometers as above. ^{13}C and ^{19}F signals are singlets unless otherwise stated. ^1H -COSY, HSQC and HMBC were used where appropriate to facilitate structural determination.

High resolution mass spectrometry data (HRMS) were obtained on an Agilent 6230 TOF LC/MS equipped with ESI detector in positive mode and on a Micromass AutoSpec Ultima Magnetic Sector instrument with EI detector in positive mode. Reaction analysis was typically performed by thin-layer chromatography on silica gel or using a Waters I-class ACQUITY UPLC-MS (Waters Corporation, Milford, MA, USA) equipped with in-line photodiode array detector (PDA), evaporative light scattering detector (ELSD) and QDa mass detector (Both ESI positive and negative ionization mode). Typically 0.1 μL sample injections were taken from acetonitrile solutions of reaction mixtures or products (\sim 1 mg/mL). A partial loop injection mode was used with the needle placement at 2.0 mm from bottom of the wells and a 0.2 μL air gap at preaspiration and postaspiration. Column used: Waters Cortecs UPLC C18+ column, 2.1 mm \times 50 mm with (Waters S5 #186007114) with Waters Cortecs UPLC C18+ VanGuard Precolumn 2.1 mm \times 5 mm (Waters #186007125), Mobile Phase A: 0.1% formic acid in Optima LC/MS-grade water, Mobile Phase B: 0.1% formic acid in Optima LC/MS-grade MeCN. Flow rate: 0.8 mL/min. Column temperature: 45 °C. The PDA sampling rate was 20 points/sec. The QDa detector monitored m/z 150–750 with a scan time of 0.06 s and a cone voltage of 30 V. The ELSD had a gain of 750, data rate of 10 pps, time constant “normal” 0.2000 s, a gas pressure of 40.0 psi, with the nebulizer in cooling mode at 75% power level and the drift tube temperature set to 50 °C. The PDA detector range was between 210 and 400 nm with a resolution of 1.2 nm. Two minute and 8 min methods were used. The method gradients are below: 2 min method, 0 min: 0.8 mL/min, 95% 0.1% formic acid in water/5% 0.1% formic acid in acetonitrile; 1.5 min: 0.8 mL/min, 0.1% 0.1% formic acid in water/99.9% 0.1% formic acid in acetonitrile; 1.91 min: 0.8 mL/min, 95% 0.1% formic acid in water/5% 0.1% formic acid in acetonitrile. Eight min method, 0 min: 0.8 mL/min, 95% 0.1% formic acid in water/5% 0.1% formic acid in acetonitrile; 7.5 min: 0.8 mL/min, 0.1% 0.1% formic acid in water/99.9% 0.1% formic acid in acetonitrile; 7.91 min: 0.8 mL/min, 95% 0.1% formic acid in water/5% 0.1% formic acid in acetonitrile.

Flash chromatography was performed on silica gel (230–400 Mesh, grade 60) under a positive pressure of Nitrogen. Thin Layer Chromatography was performed on 25 μm TLC Silica gel 60 F254 glass plates purchased from Fisher Scientific (part number: S07876). Visualization was performed using ultraviolet light (254 and 365 nm) and/or potassium permanganate (KMnO_4) stain. Reverse-phase prep-HPLC was performed on a Teledyne ISCO CombiFlash EZ Prep (RediSep Prep C18, 100 Å, 5 μm , 150 mm \times 20 mm (part no. 692203810)) using 0.1% formic acid in water and 0.1% formic acid in acetonitrile eluent.

All compounds are >95% pure by UPLC analysis.

General Procedure A Synthesis of Amide Products. A flamed-dried two-dram vial, equipped with a Teflon-coated stir bar, was charged JQ1 (40.0 mg, 0.1 mmol, 1 equiv) and PyAOP (52.1 mg, 0.1 mmol, 1 equiv). To this vial was added dry DMF (0.5 mL) followed by *N*-methyl imidazole (8.2 μL , 0.1 mmol, 1 equiv). The resulting homogeneous solution was stirred at ambient temperature for 10 min. To another flamed-dried two-dram vial was added amine HCl salt (0.1 mmol, 1 equiv) and *N*-methyl imidazole (12.3 μL , 0.15 mmol, 1.5 equiv) before the addition of DMF (0.5 mL). The amine mixture was then transferred to the first vial. The combined homogeneous solution was stirred at ambient temperature for 14 h.

Upon completion of the reaction the reaction was worked up and purified as described.

General Procedure B Synthesis of Ester Products. An oven-dried two-dram vial, equipped with a Teflon-coated stir bar, was charged with Katritzky salt (0.10 mmol, 1.0 equiv), carboxylic acid (0.10 mmol, 1.0 equiv), potassium *tert*-butoxide (11.2 mg, 0.10 mmol, 1.0 equiv), and finely ground potassium iodide (32.0 mg, 0.20 mmol, 2.0 equiv). The vial was then capped, evacuated, and refilled with N_2 three times. 1.00 mL of dioxane was added to the reaction vessel via syringe, and the reaction heated at 110 °C for 22 h at a stir rate of 500 rpm. Upon completion, the reaction was filtered through a Celite plug and washed with DCM. The filtrate was evaporated in vacuo and purified as described.

General Procedure B1 One Pot Synthesis of Ester Products. An oven-dried two-dram vial, equipped with a Teflon-coated stir bar, was charged with amine hydrochloride salt (0.10 mmol, 1.0 equiv), triphenyl pyrylium tetrafluoroborate (39.6 mg, 0.10 mmol, 1.0 equiv), carboxylic acid (0.10 mmol, 1.0 equiv), potassium *tert*-butoxide (22.4 mg, 0.20 mmol, 2.0 equiv), and finely ground potassium iodide (32.0 mg, 0.20 mmol, 2.0 equiv). The vial was then capped, evacuated, and refilled with N_2 three times. 1.00 mL of dioxane was added to the reaction vessel via syringe, and the reaction heated at 110 °C for 22 h at a stir rate of 500 rpm. Upon completion, the reaction was filtered through a Celite plug and washed with DCM. The filtrate was evaporated in vacuo and purified as described.

General Procedure C Synthesis of Alkane Products. In a nitrogen filled glovebox, an oven-dried two-dram vial, equipped with a Teflon-coated stir bar, was charged with $\text{NiBr}_2\text{-glyme}$ (12 mg, 0.04 mmol, 0.40 equiv), dtbpy (10.7 mg, 0.04 mmol, 0.40 equiv), and 800 μL of NMP (vial A). This was stirred at 500 rpm for 30 min. During this time, an oven-dried two-dram vial, equipped with a Teflon-coated stir bar, was charged with Katritzky salt (0.10 mmol, 1.0 equiv) (vial B). Another oven-dried two-dram vial, equipped with a Teflon-coated stir bar, was charged with acid (0.20 mmol, 2.0 equiv), proton sponge (42.8 mg, 0.20 mmol, 2.0 equiv), and TFFH (52.8 mg, 0.20 mmol, 2.0 equiv) (Vial C). These vials were transferred to the glovebox. Vial C had 800 μL of NMP added and was stirred for 20 min followed by addition into vial A. To vial C was added 400 μL of NMP and manganese (22 mg, 0.40 mmol, 4.0 equiv). This vial was stirred at 700 rpm for 2 min and transferred to vial A. Vial A was sealed with electrical tape, removed from the glovebox, and heated at 70 °C and 800 rpm for 14 h. Upon completion, the reaction was filtered through a pad of Celite using 30 mL of ethyl acetate. The filtrate was washed with 20 mL of saturated sodium sulfate. The organic layer was collected, dried with sodium sulfate and concentrated in vacuo. Purification was achieved as described.

General Procedure D Synthesis of Ketone Products. In a nitrogen filled glovebox, an oven-dried two-dram vial, equipped with a Teflon-coated stir bar, was charged with Nickel(II) bis-(acetylacetone) (12.5 mg, 0.04 mmol, 0.40 equiv), (Z)-*N'*-cyanopicolinimidamide (5.8 mg, 0.04 mmol, 0.40 equiv), and 800 μL of NMP (vial A). This was stirred at 500 rpm for 30 min. During this time, an oven-dried two-dram vial, equipped with a Teflon-coated stir bar, was charged with Katritzky salt (0.10 mmol, 1.0 equiv) (vial B). Another oven-dried two-dram vial, equipped with a Teflon-coated stir bar, was charged with acid (0.20 mmol, 2.0 equiv) (vial C). These vials were transferred to the glovebox. Vial C had 800 μL of NMP and dimethyldicarbonate (32.2 μL , 40.2 mg, 0.30 mmol, 3.0 equiv) and was stirred at 500 rpm for 20 min followed by addition into vial A. To vial B was added 400 μL of NMP and manganese (22 mg, 0.40 mmol, 4.0 equiv). This vial was stirred at 700 rpm for 2 min and transferred to vial A. Triethyl amine hydrochloride (28 mg, 0.20 mmol, 2.0 equiv) was added to the vial and it was capped, sealed with electrical tape, removed from the glovebox, and heated at 70 °C and 800 rpm for 14 h. Upon completion, the reaction was filtered through a pad of Celite using 30 mL of ethyl acetate. The filtrate was washed with 20 mL of saturated sodium sulfate. The organic layer was collected, dried with sodium sulfate and concentrated in vacuo. Purification was achieved as described.

General Procedure D Synthesis of Amine Products. In a nitrogen filled glovebox, an oven-dried one-dram vial, equipped with a Teflon-coated stir bar, was charged with Platinum(II) chloride (1.3 mg, 0.005 mmol, 0.05 equiv) and Brettphos (5.3 mg, 0.01 mmol, 0.01 equiv). 100 μ L of 1:1 dioxane/DMSO was added and the solution stirred for 20 min at 30 °C and 300 rpm. Outside of the glovebox, an additional oven-dried one-dram vial, equipped with a Teflon-coated stir bar, was charged with amine (0.1 mmol, 1.0 equiv) and carboxylic acid (0.15 mmol, 1.5 equiv). 900 μ L of solvent was added. The catalyst solution was removed from the glovebox, cooled to room temperature, and phenylsilane (61 μ L, 0.5 mmol, 5.0 equiv) added via syringe. Note the solution will bubble vigorously and generate hydrogen gas. The yellow solution was transferred via syringe to the amine/acid vial which was subsequently heated at 70 °C for 16 h and a stir rate of 500 rpm. Upon completion, the reaction was worked up and purified as described.

2-((S)-4-(4-Chlorophenyl)-2,3,9-trimethyl-6H-thieno[3,2-f]-[1,2,4]triazolo[4,3-a][1,4]diazepin-6-yl)-N-(4-(2-(2,6-dioxopiperidin-3-yl)-1,3-dioxoisooindolin-4-yl)oxy)acetamido)butyl)acetamide (dBet1) (3). dBet1 (compound 3) was prepared from **1** to **2** on a 0.1 mmol scale via general procedure A. Upon completion of the reaction it was quenched by the addition of 20 mL saturated aqueous Na₂SO₄ solution. The phases were then separated, and the aqueous phase was extracted with EtOAc (3 \times 20 mL). The combined organic fractions were then washed with brine then dried over MgSO₄, filtered, and concentrated in vacuo. The resulting residue was redissolved in MeCN/H₂O (3:1 mL, HPLC grade) and purified via preparative HPLC to give 57.5 mg (73%) of desired amide as a white solid. UPLC Retention time 2 min method: 0.97 min ¹H NMR (500 MHz, CD₃OD) δ 7.90 (s, 1H), 7.80 (t, J = 7.9 Hz, 1H), 7.52 (d, J = 7.3 Hz, 1H), 7.44 (td, J = 4.6, 2.2 Hz, 4H), 7.39 (dd, J = 8.7, 2.8 Hz, 2H), 5.10 (ddd, J = 12.2, 5.5, 3.1 Hz, 1H), 4.76 (s, 2H), 4.62 (dd, J = 8.9, 5.3 Hz, 1H), 3.45–3.31 (m, 9H), 3.31–3.24 (m, 2H), 2.87–2.75 (m, 1H), 2.75–2.62 (m, 6H), 2.43 (s, 3H), 2.10 (tp, J = 7.8, 3.8, 3.2 Hz, 1H), 1.75–1.55 (m, 7H). ¹³C NMR (126 MHz, CD₃OD) δ 173.1, 171.3, 169.9, 169.9, 168.5, 166.9, 166.4, 164.9, 164.8, 155.6, 154.9, 150.8, 136.8, 136.7, 136.6, 133.5, 132.1, 131.8, 130.7, 130.6, 130.6, 129.9, 128.4, 120.5, 120.5, 118.0, 116.6, 78.1, 68.2, 53.8, 38.7, 38.7, 38.4, 37.5, 30.7, 30.7, 26.4, 26.2, 22.2, 13.0, 11.5, 10.2. HRMS (ESI) Calculated C₃₈H₃₇ClN₈O₇S⁺ [M + H]⁺: 785.2267, Found 785.2268.

4-(2-((2,6-Dioxopiperidin-3-yl)-1,3-dioxoisooindolin-4-yl)oxy)acetamido)butyl 2-((S)-4-(4-chlorophenyl)-2,3,9-trimethyl-6H-thieno[3,2-f][1,2,4]triazolo[4,3-a][1,4]diazepin-6-yl)acetate (4). Compound 4 was prepared from **1** to **10** on a 0.1 mmol scale via general procedure B. Filtrate was reconstituted in acetonitrile and purified via preparative HPLC to give 42.5 mg (54%) of desired ester as an off white solid. Compound was also prepared via general procedure B1 in a one pot fashion to give 21.8 mg (28%) of desired ester. UPLC Retention time 2 min method: 1.06 min R_f 93:7 DCM/MeOH: ¹H NMR (600 MHz, DMSO) δ 10.90 (s, 1H), 7.80 (dd, J = 8.5, 7.2 Hz, 2H), 7.51–7.41 (m, 6H), 5.08 (dd, J = 12.5, 5.5 Hz, 1H), 4.75 (s, 2H), 4.50 (dd, J = 8.0, 6.3 Hz, 1H), 4.12 (qt, J = 10.9, 6.4 Hz, 2H), 3.48 (dd, J = 16.4, 6.3 Hz, 1H), 3.42 (dd, J = 16.4, 8.0 Hz, 1H), 2.88 (ddd, J = 16.8, 13.5, 5.7 Hz, 1H), 2.65–2.54 (m, 2H), 2.60 (s, 3H), 2.41 (s, 3H), 2.06 (tp, J = 7.9, 2.9 Hz, 1H), 1.67–1.59 (m, 2H), 1.64 (s, 3H), 1.52 (p, J = 6.9 Hz, 2H). ¹³C NMR (151 MHz, DMSO) δ 172.1, 170.1, 169.2, 166.4, 166.3, 165.2, 163.0, 154.9, 154.4, 149.5, 136.5, 136.4, 135.1, 132.8, 132.0, 130.5, 129.8, 129.6, 129.3, 128.2, 120.6, 116.9, 115.9, 67.9, 63.5, 53.3, 48.7, 37.7, 36.3, 30.7, 25.3, 25.2, 21.8, 13.5, 12.3, 10.8. HRMS (ESI) Calculated C₃₈H₃₇ClN₈O₇S⁺ [M + H]⁺: 786.2107, Found 786.2098.

N-(5-((S)-4-(4-Chlorophenyl)-2,3,9-trimethyl-6H-thieno[3,2-f]-[1,2,4]triazolo[4,3-a][1,4]diazepin-6-yl)pentyl)-2-((2,6-dioxopiperidin-3-yl)-1,3-dioxoisooindolin-4-yl)oxy)acetamide (5). Compound 5 was prepared from **1** to **10** on a 0.10 mmol scale via general procedure C. The crude residue was passed through a plug of silica gel to remove the triphenylpyridine. The plug was initially washed with 50 mL of DCM followed by 50 mL of 7% methanol in DCM. The methanol/DCM fraction was evaporated, reconstituted in acetonitrile and purified via preparative HPLC to give 24.5 mg (33%) of

of desired alkane product as a white solid. UPLC Retention time 4 min method: 1.77 min R_f 93:7 DCM/MeOH: 0.48 ¹H NMR (500 MHz, CDCl₃) δ 7.70 (m, 1H), 7.66 (dt, J = 8.1, 4.1 Hz, 1H), 7.47 (dd, J = 7.3, 1.8 Hz, 1H), 7.37 (dd, J = 8.6, 2.6 Hz, 2H), 7.26 (dd, J = 10.0, 8.5 Hz, 2H), 7.11 (dd, J = 8.4, 6.0 Hz, 1H), 4.86 (dt, J = 12.6, 4.6 Hz, 1H), 4.61 (dd, J = 13.9, 2.0 Hz, 1H), 4.53 (dd, J = 13.9, 11.3 Hz, 1H), 3.86 (td, J = 10.2, 4.4 Hz, 1H), 3.72–3.56 (m, 1H), 3.17 (q, J = 7.9, 7.0 Hz, 1H), 2.83–2.55 (m, 4H), 2.61 (d, J = 6.7 Hz, 3H), 2.46 (qt, J = 12.4, 4.5 Hz, 1H), 2.34 (d, J = 3.8 Hz, 3H), 2.05 (dtd, J = 10.4, 5.2, 2.8 Hz, 1H), 1.90–1.70 (m, 1H), 1.70–1.50 (m, 5H), 1.62 (s, 3H), 1.49–1.34 (m, 1H). ¹³C NMR (126 MHz, CDCl₃) δ 171.8, 171.7, 168.6, 168.4, 166.9, 166.7, 166.6, 166.2, 163.8, 156.3, 154.6, 154.6, 149.9, 137.0, 137.0, 136.8, 133.8, 132.2, 130.9, 130.7, 130.0, 129.9, 128.9, 128.8, 119.7, 119.6, 118.5, 117.5, 68.3, 68.2, 57.5, 57.3, 49.6, 49.5, 39.2, 39.0, 31.6, 31.4, 29.6, 29.4, 27.3, 27.2, 27.0, 26.9, 23.0, 14.6, 14.6, 13.3, 12.0. HRMS (ESI) Calculated C₃₇H₃₇ClN₇O₇S⁺ [M + H]⁺: 742.2209, Found 742.2207.

N-(6-((S)-4-(4-Chlorophenyl)-2,3,9-trimethyl-6H-thieno[3,2-f]-[1,2,4]triazolo[4,3-a][1,4]diazepin-6-yl)-5-oxohexyl)-2-((2,6-dioxopiperidin-3-yl)-1,3-dioxoisooindolin-4-yl)oxy)acetamide (6). Compound 6 was prepared from **1** to **10** on a 0.10 mmol scale following general procedure D. The crude residue was passed through a plug of silica gel to remove the triphenylpyridine. The plug was initially washed with 50 mL of DCM followed by 50 mL of 7% methanol in DCM. The methanol/DCM fraction was evaporated, reconstituted in acetonitrile and purified via preparative HPLC to give to give 21.3 mg (28%) of desired ketone as a white solid. UPLC Retention time 4 min method: 1.71 min R_f 93:7 DCM/MeOH: 0.42 ¹H NMR (499 MHz, CDCl₃) δ 7.74 (ddd, J = 8.9, 7.4, 2.0 Hz, 1H), 7.60 (q, J = 5.8 Hz, 1H), 7.54 (dd, J = 7.4, 2.2 Hz, 1H), 7.38 (dd, J = 8.4, 3.1 Hz, 2H), 7.32 (d, J = 8.3 Hz, 2H), 7.21 (dd, J = 8.4, 3.8 Hz, 1H), 4.97 (dd, J = 12.4, 5.4 Hz, 1H), 4.69 (dt, J = 6.7, 3.3 Hz, 1H), 4.66 (d, J = 4.8 Hz, 2H), 3.84 (ddd, J = 17.3, 6.4, 4.9 Hz, 1H), 3.68 (ddd, J = 17.4, 7.3, 4.5 Hz, 1H), 3.47 (dp, J = 12.4, 6.2 Hz, 1H), 3.38 (h, J = 6.9 Hz, 1H), 2.87–2.81 (m, 1H), 2.79 (dd, J = 9.2, 3.1 Hz, 1H), 2.78–2.72 (m, 1H), 2.72–2.68 (m, 1H), 2.66 (d, J = 2.1 Hz, 3H), 2.41 (s, 3H), 2.14 (ddd, J = 16.5, 12.2, 8.4 Hz, 1H), 1.84–1.72 (m, 3H), 1.72–1.64 (m, 5H). ¹³C NMR (126 MHz, CDCl₃) δ 208.7, 208.6, 171.1, 171.0, 168.2, 168.1, 166.8, 166.7, 166.2, 166.1, 164.1, 163.9, 155.5, 154.6, 154.6, 149.9, 149.9, 137.0, 136.7, 133.6, 132.3, 132.2, 130.9, 130.8, 130.7, 130.4, 129.8, 128.7, 119.8, 118.4, 117.4, 68.3, 53.0, 49.4, 44.4, 44.3, 43.4, 43.4, 31.4, 28.7, 28.6, 22.7, 22.6, 21.0, 20.9, 14.4, 13.1, 11.8. HRMS (ESI) Calculated C₃₈H₃₇ClN₇O₇S⁺ [M + H]⁺: 770.2158, Found 770.2147.

N-(4-((2-((S)-4-(4-Chlorophenyl)-2,3,9-trimethyl-6H-thieno[3,2-f]-[1,2,4]triazolo[4,3-a][1,4]diazepin-6-yl)ethyl)amino)butyl)-2-((2,6-dioxopiperidin-3-yl)-1,3-dioxoisooindolin-4-yl)oxy)acetamide (7). Compound 7 was prepared from **1** to **2** on a 0.1 mmol scale relative to **2** via general procedure E where solvent = DMSO. Upon completion the reaction was quenched with 1 mL of methanol, filtered through a syringe filter, and purified via preparative HPLC to give 18.1 mg (23%) of desired amine as a white solid. UPLC Retention time 2 min method: 0.82 min ¹H NMR (500 MHz, DMSO) δ 11.12 (s, 1H), 8.55 (s, 2H), 8.05 (t, J = 5.7 Hz, 1H), 7.82 (dd, J = 8.5, 7.3 Hz, 1H), 7.50 (d, J = 5.3 Hz, 5H), 7.40 (dd, J = 8.7, 3.4 Hz, 1H), 5.15–5.07 (m, 1H), 4.79 (s, 2H), 4.32 (dd, J = 7.6, 6.0 Hz, 1H), 3.42–3.33 (m, 1H), 3.31–3.23 (m, 1H), 3.20 (q, J = 6.6 Hz, 2H), 3.03 (dt, J = 14.0, 7.1 Hz, 2H), 2.90 (ddd, J = 16.3, 14.0, 5.4 Hz, 2H), 2.77–2.63 (m, 3H), 2.61 (s, 3H), 2.46–2.35 (m, 3H), 2.08–1.99 (m, 1H), 1.71–1.58 (m, 5H), 1.53 (dq, J = 14.1, 6.9 Hz, 2H). ¹³C NMR (126 MHz, DMSO) δ 172.8, 169.9, 166.9, 166.7, 165.5, 163.7, 158.2, 158.0, 155.1, 155.0, 149.9, 137.0, 136.8, 135.3, 133.1, 132.4, 130.6, 130.3, 130.0, 129.6, 128.5, 120.5, 117.5, 116.8, 116.1, 67.7, 53.9, 48.8, 46.6, 44.2, 37.8, 30.9, 28.1, 26.2, 23.1, 22.0, 14.1, 12.6, 11.3. HRMS (ESI) Calculated C₃₈H₄₀ClN₈O₇S⁺ [M + H]⁺: 771.2475, Found 771.2469.

(2S,4R)-N-(2-(3-((2-((S)-4-(4-Chlorophenyl)-2,3,9-trimethyl-6H-thieno[3,2-f]-[1,2,4]triazolo[4,3-a][1,4]diazepin-6-yl)ethyl)amino)ethoxy)propoxy)-4-(4-methylthiazol-5-yl)benzyl)-4-hydroxy-1-((S)-3-methyl-2-(1-oxoisooindolin-2-yl)butanoyl)pyrrolidine-2-carboxamide (19). Compound 19 was prepared from **1**

to **13** on a 0.10 mmol scale relative to **13** via general procedure E where solvent = 95:5 dioxane/DMSO. Upon completion, the reaction mixture was concentrated in vacuo and redissolved in acetonitrile (3 mL, HPLC grade) then purified via preparative HPLC to 23 mg (22%) of desired amine. UPLC Retention time 2 min method: 0.93 min ¹H NMR (400 MHz, DMSO) δ 8.27 (s, 1H), 8.07 (t, J = 5.6 Hz, 1H), 7.72 (d, J = 7.5 Hz, 1H), 7.64–7.58 (m, 1H), 7.50 (dt, J = 7.9, 4.0 Hz, 1H), 7.46 (s, 3H), 7.35 (d, J = 7.6 Hz, 1H), 7.00 (d, J = 8.3 Hz, 1H), 4.75 (d, J = 10.6 Hz, 1H), 4.57 (d, J = 18.0 Hz, 1H), 4.46 (q, J = 9.7, 8.4 Hz, 2H), 4.36 (d, J = 4.5 Hz, 1H), 4.31 (dd, J = 11.8, 5.8 Hz, 2H), 4.13 (ddt, J = 20.2, 13.7, 6.6 Hz, 3H), 3.79 (dd, J = 10.5, 4.8 Hz, 1H), 3.68 (d, J = 10.3 Hz, 1H), 3.59 (t, J = 6.3 Hz, 1H), 3.56–3.44 (m, 2H), 2.75 (t, J = 6.1 Hz, 1H), 2.59 (s, 3H), 2.56–2.42 (m, 9H), 2.41–2.32 (m, 3H), 2.24 (s, 1H), 2.08–1.91 (m, 4H), 1.64 (s, 3H), 0.97 (d, J = 6.5 Hz, 3H), 0.77 (d, J = 6.7 Hz, 3H). ¹³C NMR (151 MHz, DMSO) δ 171.6, 168.1, 167.5, 163.2, 155.9, 155.4, 151.5, 149.7, 147.9, 142.2, 136.9, 135.2, 134.1, 132.3, 131.6, 131.4, 131.3, 131.0, 130.5, 130.2, 129.9, 129.6, 128.5, 127.9, 127.8, 127.2, 127.0, 123.6, 123.0, 120.9, 111.7, 79.2, 68.6, 66.9, 64.8, 58.7, 57.8, 55.4, 54.3, 48.0, 46.8, 45.3, 42.7, 38.1, 37.1, 29.0, 28.4, 18.9, 18.6, 16.0, 14.1, 14.0, 12.7, 11.3. HRMS (ESI) Calculated C₅₃H₆₁ClN₉O₆S₂⁺ [M + H]⁺: 1018.3869, Found 1018.3862.

tert-Butyl 4-((2-((4S,6R)-6-(2-(2-(4-fluorophenyl)-5-isopropyl-3-phenyl-4-(phenylcarbamoyl)-1H-pyrrol-1-yl)ethyl)-2,2-dimethyl-1,3-dioxan-4-yl)ethyl)amino)piperidine-1-carboxylate (**20**). Compound **20** was prepared from **17** and **15** on a 0.100 mmol scale relative to **15** via general via general procedure E on where solvent = 3:7 DMSO/dioxane. When the reaction was complete after 5 h, it was cooled to room temperature and diluted with 30 mL of saturated sodium bicarbonate solution. This was extracted with DCM (3 × 25 mL). The organic layers were combined, washed with 30 mL of saturated sodium sulfate, dried over sodium sulfate, and concentrated. The residue was reconstituted in acetonitrile and purified via prep HPLC to give 28.4 mg (37%) of the desired amine as a white solid. UPLC Retention time 2 min method: 1.12 min ¹H NMR (499 MHz, CDCl₃) δ 7.16 (dt, J = 12.3, 7.4 Hz, 9H), 7.06 (d, J = 8.0 Hz, 2H), 6.98 (td, J = 8.1, 7.5, 4.7 Hz, 3H), 6.85 (s, 1H), 4.08 (m, 4H), 3.89–3.76 (m, 3H), 3.65 (dd, J = 7.8, 4.6 Hz, 1H), 3.56 (p, J = 7.1 Hz, 1H), 2.84 (dq, J = 6.8, 4.1, 2.9 Hz, 2H), 2.81–2.66 (m, 3H), 1.91 (d, J = 12.7 Hz, 2H), 1.68 (q, J = 6.8 Hz, 3H), 1.52 (d, J = 7.1 Hz, 6H), 1.44 (s, 9H), 1.39 (d, J = 11.8 Hz, 2H), 1.33 (s, 3H), 1.29 (s, 3H), 1.22 (dt, J = 12.9, 2.5 Hz, 1H), 1.06 (q, J = 11.9 Hz, 1H). ¹³C NMR (126 MHz, CDCl₃) δ 164.9, 162.4 (d, J = 247.8 Hz), 154.8, 141.6, 138.5, 134.8, 133.3 (d, J = 8.0 Hz), 130.6, 128.9 (d, J = 10.4 Hz), 128.5, 126.7, 123.7, 119.7, 115.5 (d, J = 21.5 Hz), 98.7, 79.9, 66.6, 55.0, 42.3, 41.0, 38.2, 36.4, 30.2, 28.6, 28.5, 26.2, 21.9, 21.8, 20.0. ¹⁹F NMR (470 MHz, CDCl₃) δ -113.73. HRMS (ESI) Calculated C₄₆H₆₀FN₄O₅⁺ [M + H]⁺: 767.4542, Found 767.4539

tert-Butyl 4-((2-(1-(4-chlorobenzoyl)-5-methoxy-2-methyl-1H-indol-3-yl)ethyl)amino)piperidine-1-carboxylate (**21**). Compound **21** was prepared from **16** (indomethacin) and **15** via general procedure E on a 0.20 mmol scale where solvent = 3:7 DMSO/dioxane. When the reaction was complete after 3 h, it was cooled to room temperature and diluted with 30 mL of saturated sodium bicarbonate solution. This was extracted with DCM (3 × 25 mL). The organic layers were combined, washed with 30 mL of saturated sodium sulfate, dried over sodium sulfate, and concentrated. The resulting residue was purified by column chromatography using DCM/acetone/meOH to give 35.0 mg (33%) of the desired amine as a yellow oil. The purified material had 20 μ L of trifluoroacetic acid added to the NMR sample. UPLC Retention time 2 min method: 0.98 min ¹H NMR (499 MHz, cd₃cn) δ 7.68–7.64 (m, 2H), 7.58–7.55 (m, 2H), 7.10 (d, J = 2.5 Hz, 1H), 6.99 (d, J = 9.0 Hz, 1H), 6.71 (dd, J = 9.0, 2.5 Hz, 1H), 4.12 (d, J = 13.7 Hz, 2H), 3.84 (s, 3H), 3.38–3.29 (m, 1H), 3.28–3.19 (m, 2H), 3.11–3.04 (m, 2H), 2.73 (d, J = 11.2 Hz, 2H), 2.29 (s, 3H), 2.03 (d, J = 11.9 Hz, 2H), 1.51 (qd, J = 12.3, 4.5 Hz, 2H), 1.43 (s, 9H). ¹³C NMR (126 MHz, cd₃cn) δ 169.4, 158.7, 158.3, 157.2, 155.4, 139.7, 137.0, 135.3, 132.2, 132.1, 130.1, 117.0, 116.1, 114.7, 112.4, 102.2, 80.7, 57.5, 56.4, 45.5, 29.1,

28.5, 21.8, 13.7. ¹⁹F NMR (470 MHz, cd₃cn) δ -76.86. HRMS (ESI) Calculated C₂₉H₃₇ClN₃O₄⁺ [M + H]⁺: 526.2467, Found 526.2469.

1-5-(4-((2-(1,8-Diethyl-1,3,4,9-tetrahydropyranol[3,4-*b*]indol-1-yl)ethyl)amino)hexanoyl)piperazine-1-carboxylate-2-methylphenyl)dihydropyrimidine-2,4(1H,3H)-dione (**22**). Compound **22** was prepared from **18** (etodolac) and **11** on a 0.100 mmol scale relative to **11** via general via general procedure E on where solvent = 3:7 DMSO/dioxane. When the reaction was complete after 5 h, it was cooled to room temperature and diluted with 30 mL of saturated sodium bicarbonate solution. This was extracted with DCM (3 × 25 mL). The organic layers were combined, washed with 30 mL of saturated sodium sulfate, dried over sodium sulfate, and concentrated. The residue was reconstituted in acetonitrile and purified via prep HPLC to give 15.3 mg (23%) of the desired amine as a white solid. UPLC Retention time 2 min method: 0.85 min ¹H NMR (499 MHz, CDCl₃) δ 10.75 (s, 1H), 8.61 (s, 1H), 7.36 (d, J = 7.9 Hz, 1H), 7.31 (d, J = 8.9 Hz, 3H), 7.04 (t, J = 7.4 Hz, 1H), 6.99 (d, J = 7.1 Hz, 1H), 4.09–4.02 (m, 1H), 3.96 (td, J = 11.0, 3.8 Hz, 1H), 3.85–3.78 (m, 1H), 3.78–3.29 (m, 9H), 2.95 (td, J = 15.8, 15.2, 7.8 Hz, 2H), 2.85 (ddt, J = 15.6, 12.4, 7.9 Hz, 6H), 2.76–2.66 (m, 2H), 2.53 (dd, J = 12.7, 6.5 Hz, 1H), 2.31 (s, 3H), 2.27–2.21 (m, 1H), 2.17 (s, 1H), 2.13 (d, J = 7.3 Hz, 1H), 2.03 (dt, J = 14.9, 7.5 Hz, 1H), 1.90 (dq, J = 14.8, 7.4 Hz, 1H), 1.39 (p, J = 7.3 Hz, 3H), 1.32 (d, J = 7.6 Hz, 3H), 0.97 (t, J = 7.4 Hz, 4H). ¹³C NMR (126 MHz, CDCl₃) δ 171.6, 169.7, 168.7, 139.9, 138.4, 136.6, 135.3, 133.5, 131.4, 128.2, 127.1, 126.6, 126.5, 121.8, 120.7, 119.4, 115.7, 108.5, 75.8, 60.5, 47.6, 45.21, 44.71, 33.5, 32.5, 31.6, 31.5, 25.7, 25.6, 24.2, 23.7, 22.5, 18.1, 14.4, 8.0. HRMS (ESI) Calculated C₃₉H₅₃N₆O₅⁺ [M + H]⁺: 685.4072, Found 685.4067.

(2*S*,4*R*)-N-(2-(3-(2-(2-((4-Chlorophenyl)-2,3,9-trimethyl-6H-thieno[3,2-f][1,2,4]triazolo[4,3-a][1,4]diazepin-6-yl)acetamido)-ethoxy)propoxy)-4-(4-methylthiazol-5-yl)benzyl)-4-hydroxy-1-(*S*-3-methyl-2-(1-oxoisindolin-2-yl)butanoyl)pyrrolidine-2-carboxamide (**23**). Compound **23** was prepared from **1** to **13** on a 0.10 mmol scale following general procedure A. Upon completion the reaction was quenched by the addition of 20 mL saturated aqueous NaHCO₃ solution. The phases were then separated, and the aqueous phase was extracted with EtOAc (3 × 20 mL). The combined organic fractions were then washed with brine then dried over MgSO₄, filtered, and concentrated in vacuo. The resulting residue was redissolved in MeCN (3 mL, HPLC grade) and purified via preparative HPLC to give 48.5 mg (47%) of desired amide as a white solid. R_f = 0.37 (10% MeOH/DCM) UPLC Retention time 2 min method: 1.13 min ¹H NMR (500 MHz, CDCl₃) δ 8.66 (s, 1H), 7.78 (s, 1H), 7.49 (t, J = 7.5 Hz, 1H), 7.41–7.33 (m, 5H), 7.30 (d, J = 7.9 Hz, 3H), 7.02 (m, 1H), 6.96 (d, J = 7.6 Hz, 1H), 6.92 (s, 1H), 4.79 (d, J = 10.8 Hz, 1H), 4.72–4.65 (m, 2H), 4.62–4.51 (m, 2H), 4.46 (dd, J = 14.7, 5.5 Hz, 1H), 4.37 (d, J = 17.5 Hz, 1H), 4.28 (d, J = 11.2 Hz, 1H), 4.14 (td, J = 11.7, 6.7 Hz, 2H), 3.72 (dh, J = 21.3, 6.1 Hz, 3H), 3.58 (d, J = 5.7 Hz, 2H), 3.47 (q, J = 5.5 Hz, 3H), 3.28 (dd, J = 14.6, 6.3 Hz, 1H), 2.56 (s, 4H), 2.52–2.43 (m, 8H), 2.39 (s, 4H), 2.14 (s, 1H), 1.65 (s, 3H), 1.30–1.22 (m, 1H), 0.92 (d, J = 6.5 Hz, 3H), 0.85 (d, J = 6.6 Hz, 3H). ¹³C NMR (126 MHz, CDCl₃) δ 170.7, 170.2, 163.9, 156.9, 142.2, 136.9, 136.7, 131.8, 131.7, 131.0, 130.6, 129.9, 129.7, 128.8, 128.0, 126.5, 123.9, 122.9, 121.8, 112.4, 69.9, 69.5, 67.7, 65.2, 58.8, 58.7, 55.9, 47.4, 39.6, 39.2, 39.1, 36.4, 29.8, 29.5, 29.0, 19.2, 19.0, 16.3, 14.5, 13.2, 11.8. HRMS (ESI) Calculated C₅₃H₅₅ClN₉O₇S₂⁺ [M + H]⁺: 1032.3662, Found 1032.3660.

2-3-((2-((2*S*,4*R*)-4-Hydroxy-1-((*S*)-3-methyl-2-(1-oxoisindolin-2-yl)butanoyl)pyrrolidine-2-carboxamido)methyl)-5-(4-methylthiazol-5-yl)phenoxy)propoxyethyl 2-((4-(4-chlorophenyl)-2,3,9-trimethyl-6H-thieno[3,2-f][1,2,4]triazolo[4,3-a][1,4]diazepin-6-yl)-acetate (**24**). Compound **24** was prepared from **1** to **13a** on a 0.10 mmol scale via general procedure B. Filtrate was purified by flash chromatography on silica gel using DCM/Acetone (50%) to MeOH/DCM (10%) as eluent to 34.0 mg (36%) of desired ester as a white solid. Compound **24** was also prepared from **1** to **13** on a 0.10 mmol scale via general procedure B1 to give 25.8 mg (25%). R_f = 0.50 (10% MeOH/DCM) UPLC Retention time 2 min method: 1.21 min ¹H NMR (500 MHz, CDCl₃) δ 8.68 (s, 1H), 7.75–7.71 (m, 1H), 7.48 (td, J = 7.4, 1.1 Hz, 1H), 7.42–7.34 (m, 5H), 7.29 (dd, J = 8.3, 1.9

Hz, 3H), 6.93 (dd, J = 7.6, 1.6 Hz, 1H), 6.89 (d, J = 1.7 Hz, 1H), 4.76 (d, J = 10.9 Hz, 1H), 4.73–4.66 (m, 2H), 4.58–4.49 (m, 3H), 4.46 (dd, J = 15.0, 5.8 Hz, 1H), 4.40–4.32 (m, 3H), 4.26 (ddd, J = 11.8, 6.0, 3.7 Hz, 1H), 4.14 (t, J = 6.0 Hz, 2H), 3.78–3.68 (m, 5H), 3.62–3.51 (m, 2H), 2.61 (s, 3H), 2.51 (s, 3H), 2.46 (m, 1H), 2.39 (s, 3H), 2.18–2.09 (m, 3H), 1.66 (s, 3H), 0.93 (d, J = 6.5 Hz, 3H), 0.85 (d, J = 6.5 Hz, 3H). ^{13}C NMR (126 MHz, CDCl_3) δ 170.7, 170.2, 163.9, 156.9, 142.2, 136.9, 136.7, 131.8, 131.7, 131.0, 130.6, 129.9, 129.7, 128.8, 128.0, 126.5, 123.9, 122.9, 121.8, 112.4, 69.9, 69.5, 67.7, 65.2, 58.8, 58.7, 55.9, 47.4, 39.6, 39.2, 39.1, 36.4, 29.8, 29.5, 29.0, 19.2, 19.0, 16.3, 14.5, 13.2, 11.8. HRMS (ESI) Calculated $\text{C}_{53}\text{H}_{58}\text{ClN}_8\text{O}_8\text{S}_2^+ [\text{M} + \text{H}]^+$: 1033.3502, Found 1033.3502.

(2S,4R)-*N*-(2-(3-(4-((S)-4-(4-Chlorophenyl)-2,3,9-trimethyl-6H-thieno[3,2-f][1,2,4]triazolo[4,3-a][1,4]diazepin-6-yl)butoxy)-propoxy)-4-(4-methylthiazol-5-yl)benzyl)-4-hydroxy-1-(S)-3-methyl-2-(1-oxoisooindolin-2-yl)butanoyl)pyrrolidine-2-carboxamide (**25**). Compound **25** was prepared from **1** to **13a** on a 0.10 mmol scale following general procedure C. The product was purified via preparative HPLC to 21 mg (20%) of desired alkane product as a white solid. UPLC Retention time 8 min method: 4.19 min ^1H NMR (400 MHz, cd_3cn) δ 8.71 (s, 1H), 7.70 (d, J = 7.5 Hz, 1H), 7.61–7.40 (m, 6H), 7.38–7.33 (m, 2H), 7.31 (d, J = 8.0 Hz, 1H), 7.25 (t, J = 6.1 Hz, 1H), 6.98 (d, J = 1.9 Hz, 1H), 4.74 (d, J = 10.9 Hz, 1H), 4.57 (d, J = 17.8 Hz, 1H), 4.48–4.41 (m, 2H), 4.39–4.34 (m, 4H), 4.11 (t, J = 6.1 Hz, 2H), 3.97 (dd, J = 8.4, 5.9 Hz, 1H), 3.86 (d, J = 10.9 Hz, 1H), 3.75 (dd, J = 10.9, 4.3 Hz, 1H), 3.64 (t, J = 6.1 Hz, 2H), 3.58 (td, J = 6.4, 3.2 Hz, 2H), 3.37 (d, J = 4.1 Hz, 1H), 2.54 (s, 2H), 2.45 (s, 3H), 2.40 (td, J = 7.8, 2.5 Hz, 1H), 2.35 (s, 3H), 2.15 (s, 3H), 2.06 (td, J = 12.6, 5.5 Hz, 4H), 1.86–1.73 (m, 1H), 1.62 (s, 3H), 0.92 (d, J = 6.5 Hz, 3H), 0.76 (d, J = 6.7 Hz, 3H). ^{13}C NMR (126 MHz, CD_3CN) δ 172.3, 170.2, 169.1, 164.4, 157.7, 157.0, 151.6, 150.8, 149.4, 143.5, 138.4, 136.7, 133.7, 132.9, 132.8, 132.5, 131.5, 131.4, 131.1, 129.7, 129.3, 128.8, 127.9, 124.3, 124.0, 122.0, 113.1, 79.2, 71.6, 70.5, 67.9, 66.3, 60.0, 59.3, 57.7, 56.4, 48.0, 39.0, 38.4, 30.4, 29.7, 27.3, 21.1, 19.4, 19.0, 16.5, 14.6, 13.1 HRMS (ESI) Calculated $\text{C}_{52}\text{H}_{58}\text{ClN}_8\text{O}_6\text{S}_2^+ [\text{M} + \text{H}]^+$: 989.3604, Found 989.3594.

(2S,4R)-*N*-(2-(3-(4-((S)-4-(4-Chlorophenyl)-2,3,9-trimethyl-6H-thieno[3,2-f][1,2,4]triazolo[4,3-a][1,4]diazepin-6-yl)-3-oxobutoxy)-propoxy)-4-(4-methylthiazol-5-yl)benzyl)-4-hydroxy-1-(S)-3-methyl-2-(1-oxoisooindolin-2-yl)butanoyl)pyrrolidine-2-carboxamide (**26**). Compound **26** was prepared from **1** to **13a** on a 0.95 mmol scale following a modified general procedure D where saturated sodium sulfate was replaced with saturated sodium bicarbonate to remove residual **1**. The crude residue was passed through a plug of silica gel to remove the triphenylpyridine. The plug was initially washed with 50 mL of DCM followed by 50 mL of 10% methanol in DCM. The methanol/DCM fraction was evaporated, reconstituted in acetonitrile and purified via preparative HPLC to give 18.6 mg (19%) of desired ketone as a white solid. UPLC Retention time 2 min method: 4.01 min ^1H NMR (499 MHz, CDCl_3) δ 8.66 (s, 1H), 7.77 (d, J = 7.2 Hz, 1H), 7.50 (td, J = 7.3, 1.1 Hz, 1H), 7.42 (d, J = 8.0 Hz, 2H), 7.41–7.25 (m, 8H), 6.92 (dd, J = 7.6, 1.6 Hz, 1H), 6.84 (d, J = 1.6 Hz, 1H), 4.76 (d, J = 10.9 Hz, 1H), 4.72–4.63 (m, 2H), 4.56 (t, J = 7.5 Hz, 1H), 4.55–4.49 (m, 1H), 4.48 (dd, J = 5.9, 4.0 Hz, 2H), 4.40–4.34 (m, 2H), 4.10 (t, J = 6.1 Hz, 2H), 3.84 (t, J = 6.4 Hz, 1H), 3.79–3.58 (m, 5H), 3.48 (s, 1H), 2.99 (dt, J = 16.5, 6.2 Hz, 1H), 2.88 (dt, J = 16.5, 6.5 Hz, 1H), 2.69–2.65 (m, 1H), 2.57 (s, 3H), 2.54–2.45 (m, 1H), 2.49 (s, 3H), 2.41 (td, J = 7.9, 7.1, 3.7 Hz, 2H), 2.38 (s, 3H), 2.17–2.05 (m, 3H), 1.72–1.65 (m, 1H), 1.64 (s, 3H), 0.91 (d, J = 6.5 Hz, 3H), 0.86 (d, J = 6.6 Hz, 3H). ^{13}C NMR (126 MHz, CDCl_3) δ 207.2, 170.8, 170.2, 169.4, 164.0, 156.9, 155.5, 150.3, 148.5, 142.3, 136.9, 136.8, 131.9, 131.8, 131.0, 130.9, 130.5, 129.9, 129.6, 128.8, 128.0, 126.5, 123.9, 123.0, 121.6, 112.1, 76.9, 70.2, 67.6, 65.8, 65.0, 58.7, 56.0, 52.8, 47.5, 44.8, 44.1, 39.1, 36.3, 29.7, 28.9, 19.2, 19.1, 16.2, 14.5, 13.2, 11.8. HRMS (ESI) Calculated $\text{C}_{53}\text{H}_{58}\text{ClN}_8\text{O}_7\text{S}_2^+ [\text{M} + \text{H}]^+$: 1017.3553, Found 1017.3559.

HTRF BRD4 Degradation and CellTiter-Glo (CTG) Assays. The HTRF and CellTiter-Glo (CTG) assays were conducted simultaneously using HEK293, cultured in 90% (v/v) DMEM (Gibco, 11995-065) with 10% (v/v) Fetal Bovine Serum (16000-044). The HTRF total BRD4 detection kit and CellTiter-Glo (CTG)

kit were sourced at Revvity (64BRD4TPEH) and Promega (G7571), respectively. The HEK293 cells were harvested at 90% confluence and then resuspended at the density of 1×10^6 cells per mL in 99% DMEM with 1% (v/v) Fetal Bovine Serum. In a 1536-well assay plate (Corning, 9145BC), 5 nL of serial-diluted compounds were dispensed into 4.5 μL of cells per each well. The plates were incubated at 37 °C with 5% CO₂ for 24 h. For the HTRF assay, 1.5 μL of 1×HTF lysis buffer was added to each well. After incubation at room temperature for 1 h, 1.5 μL of detection buffer (1:40 (v/v) dilution for both Eu cryptate and D2 antibodies) was added into each well. The reaction was further incubated for overnight at room temperature before plate reading by PHERAstar FSX using HTRF filter, channel A 337/665, (60/400), channel B 337/620 (60/400). For the CTG assay, 4.5 μL of 1×CTG solution was added to each well and the assay plate was incubated in dark at room temperature for 20 min to stabilize luminescent signal. The CTG signals were then measured by PHERAstar FSX using LUM plus setting.

BRD4-BD1 Domain Biochemical Binding Assay. The HTRF biochemical assay is used to determine the binding affinity of the tested BRD4 binding molecules to the BRD4 bromodomain 1 (BD1). This assay measures the activity of tested compounds of the binding between N-terminal GST-tagged BRD4-BD1 domain and a synthetic biotinylated histon4 peptide ([Lys(S,8,12,16)Ac]-H4(1–21)-biotin, AnaSpec, 64989) from human histone H4. In a 384-well white small-volume plate (PerkinElmer, 6008289), 10 nL of serial-diluted compounds were dispensed into 5 μL binding domain diluent buffer (PerkinElmer, 62DLBDDF). Subsequently, both GST-tagged BRD4-BD1 protein and biotinylated BRD4 binding peptide were added to the 10 mM and the mixture was incubated for 30 min at room temperature. The equilibrated protein-peptide complexes were then mixed with 5 μL of detection buffer (CisBio, 62DB1FDG) containing 10 nM anti-GST-Eu3+ (CisBio, 61H12TLB) and 2.5 nM Streptavidin-D2 (CisBio, 610SADLB). After 3 h of incubation at room temperature, the plates were measured in a PheraStar reader FSX (BMG Labtech) using the homogeneous time-resolved fluorescence (HTRF) optical module (excitation: 337 nm with 10 flashes; emission: 620 and 665 nm). The compound activity AC₅₀ values were calculated by fitting the data to the equation “log(inhibitor) vs response – variable slope” using the GraphPad Prism software.

Cellular NanoBRET Target Engagement Assay. The cellular NanoBRET target engagement assay for VHL and CRBN was obtained from Promega (Promega N2912, N2932). The assays were conducted following the manufacturer's technical manual with minor modifications. HEK293 cells were transiently transfected with the NanoLuc-CRBN or NanoLuc-VHL fusion vector using the FuGENE transfection kit (Promega E5911). After 24 h of incubation at 37 °C with 5% CO₂, the cell lines were harvested and stored in liquid nitrogen. To analyze target engagement for CRBN and VHL E3 ligases, these two cell lines were resuspended in Opti-Mem medium (Gibco 11058-021) at a density of 5×10^5 cells per mL and dispensed into a 384-well plate (Corning 3574). For live cell NanoBRET measurement, these cell lines were treated with 0.5 μM (CRBN) or 1 μM (VHL) tracer and serially diluted unlabeled PROTAC compounds for 2 h incubation at 37 °C with 5% CO₂. In the permeabilized condition, before digitonin treatment (50 $\mu\text{g}/\text{mL}$) for 30 min, NanoLuc-CRBN or NanoLuc-VHL expressing cell lines were dosed with 0.15 μM (CRBN) or 0.25 μM (VHL) tracer and serially diluted unlabeled PROTAC compounds. Thereafter, both live and permeabilized cells were treated with 1× Nano-Glo substrate for 3 min (supplemented with 1× NanoLuc-extracellular inhibitor only for the live cell condition). The BRET signals were collected using a PHERAstar FSX with the LUM 2007H1 module (610-LP, 450–480 nM).

BRD4-PROTAC-CRBN Ternary Complex Formation HTRF Assay. The BRD4-PROTAC-CRBN ternary complex assay allows for the quantitative evaluation of the activity of tested compounds in bridging the interaction between the N-terminal GST-tagged BRD4-BD1 domain (BPS, 31040) and the biotinylated CRBN/DDB1 protein complex (prepared internally). In a 384-well white small-

volume plate (PerkinElmer, 6008289), 20 nL of 2-fold serial-diluted compounds (Top concentration: 10 mM) were dispensed into each well in columns 1–22, with columns 23–24 containing 20 nL of positive control (dBET6, final concentration: 98 nM) and DMSO, respectively. The 2× protein mixture was prepared by combining the following components in the Binding Domain Diluent Buffer (Revvity, 62DLBDDF): 20 nM GST-tagged BRD4-BD1 domain and 200 nM CRBN/DDB1 protein complex. Subsequently, 5 μL of the 2× protein mixture was added to each well, and the plate was incubated at room temperature for 1 h. To create the 2× detection solution, the anti-GST Eu3+ antibody (Revvity, 61HI2TLB) and streptavidin-*d*₂ (Revvity, 610SADLB) were diluted with the Binding Domain Detection Buffer (Revvity, 62DB1FDG) to 2 and 100 nM, respectively. Following this, 5 μL of the detection solution was added to each well, and the plate was incubated at room temperature for 3 h before reading in a PheraStar reader FSX (BMG Labtech) using the homogeneous time-resolved fluorescence (HTRF) optical module (excitation: 337 nm with 10 flashes; emission: 620 and 665 nm). The BRD4-PROTAC-CRBN ternary complex formation EC₅₀, ternary complex inhibition EC₅₀, peak *B*_{max} value and area under the curve (AUC) values were determined by fitting the data to the nonlinear bell-shaped curve model using GraphPad Prism software.

Computational Modeling Methods. Molecular modeling studies utilized the crystal structure of Cereblon bound to BRD4-BD1 and DDB1 protein in complex with dBET6 PROTAC (PDB entry 6BOY).⁵⁵ DDB1 and Cereblon proteins were removed from the crystal structure and the remaining complex (BRD4 bound to dBET6) was prepared using standard Protein Preparation module of Schrödinger suite (version 2023).⁵⁶ Compounds 3 (amide), 4 (ester), and 7 (amine) were prepared using the Ligprep module, and the corresponding OPLS force-field parameters were calculated. Initial models were generated by aligning compounds 3, 4, and 7 to the bound dBET6 compound in the BRD4 crystal structure and subsequently replacing the dBET6 ligand to create three models. MD simulation was performed using Desmond MD engine (Schrödinger suite).⁵⁷ Models were solvated using SPC solvent models and relaxed using standard minimization protocol in Maestro. The finalized system underwent a 250 ns MD simulation, with coordinates saved at intervals of 25 ps. Conformational analysis was then performed on the resulting trajectory to gain insights into the dynamic properties of the system.

■ ASSOCIATED CONTENT

Data Availability Statement

Data Availability Statement Code used to generate the tSNE as well as the potency graphics, SMILES strings of all enumerated products, and an interactive version of the tSNE are available at <https://github.com/cernak-lab/cernak-lab.github.io/tree/main/publications/McGrath%20Diverse%20Amine-Acid%20Couplings%20PROTACs>.

SI Supporting Information

The Supporting Information is available free of charge at <https://pubs.acs.org/doi/10.1021/acs.jmedchem.4c02047>.

6BOY_model_amine (PDB)

6BOY_model_amide (PDB)

6BOY_model_est (PDB)

Experimental procedures; characterization data; copies of all spectral data; and further discussion (PDF)

Bio data (CSV)

■ AUTHOR INFORMATION

Corresponding Authors

Christine F. Gelin – Therapeutics Discovery, Janssen Research & Development, LLC, La Jolla, California 92121, United States; orcid.org/0000-0001-5917-3588; Email: cgegin@its.jnj.com

Tim Cernak – Department of Medicinal Chemistry, University of Michigan, Ann Arbor, Michigan 48104, United States; orcid.org/0000-0001-5407-0643; Email: tcernak@med.umich.edu

Authors

Andrew McGrath – Department of Medicinal Chemistry, University of Michigan, Ann Arbor, Michigan 48104, United States; orcid.org/0000-0001-9275-0017

Haiyan Huang – Department of Medicinal Chemistry, University of Michigan, Ann Arbor, Michigan 48104, United States

Jean-Francois Brazeau – Therapeutics Discovery, Janssen Research & Development, LLC, La Jolla, California 92121, United States

Zirong Zhang – Department of Medicinal Chemistry, University of Michigan, Ann Arbor, Michigan 48104, United States

Christopher O. Audu – Department of Medicinal Chemistry, University of Michigan, Ann Arbor, Michigan 48104, United States

Nadeem A. Vellore – Therapeutics Discovery, Janssen Research & Development, LLC, La Jolla, California 92121, United States

Lu Zhu – Therapeutics Discovery, Janssen Research & Development, LLC, Spring House, Pennsylvania 19477, United States

Zhicai Shi – Therapeutics Discovery, Janssen Research & Development, LLC, Spring House, Pennsylvania 19477, United States

Jennifer D. Venable – Therapeutics Discovery, Janssen Research & Development, LLC, La Jolla, California 92121, United States

Complete contact information is available at:

<https://pubs.acs.org/10.1021/acs.jmedchem.4c02047>

Author Contributions

The manuscript was written through contributions of all authors. All authors have given approval to the final version of the manuscript.

Funding

This work was funded by Janssen Therapeutics, the Alfred P. Sloan Foundation, and NIH-R01GM144471 (T.C.).

Notes

The authors declare the following competing financial interest(s): The authors declare the following competing financial interest(s): The Cernak Lab has received research funding or in-kind donations from MilliporeSigma, Relay Therapeutics, Janssen Therapeutics, SPT Labtech, AbbVie, Entos, Inc. and Merck & Co., Inc. T.C. holds equity in Scorpion Therapeutics and is a co-Founder and equity holder of Iambic Therapeutics (formerly Entos, Inc.).

■ ACKNOWLEDGMENTS

We would like to thank Paige Stout and Marcus Gutierrez for purification (reverse phase HPLC) of select compounds and Deszra Shariff for NMR analysis of select compounds. We thank Charu Chaudhry for helpful discussions during the preparation of the manuscript.

■ ABBREVIATIONS USED

AUC, area under the bell-shaped curve; BCF, tris(pentafluorophenyl)borane; BRET, bioluminescence resonance energy transfer; Bu₂O, dibutyl ether; CBN, cereblon; CTG, CellTiter-Glo; DIPEA, *N,N*-diisopropylethylamine; DMDC, dimethyl dicarbonate; dtbpy, 4,4-ditert-butylbipyridine; HBA, hydrogen bond acceptor; HBD, hydrogen bond donor; HTE, high throughput experimentation; HTRF, homogeneous time resolved fluorescence; KI, potassium iodide; KBr, potassium bromide; KTF, ternary complex peak formation AC50 values; ADME, absorption, distribution, metabolism and excretion; NaI, sodium iodide; NiBr₂•DME, nickel(II) bromide·glyme; Ni(acac)₂, nickel(II) acetylacetone; NEt₃•HCl, triethylammonium hydrochloride; POI, protein of interest; PROTAC, proteolysis targeting chimera; PSA, polar surface area; pyCamCN, (Z)-*N*-cyanopicolinimide; RBA, relative binding affinity; RMSF, root-mean-square fluctuation; tSNE, t-distributed stochastic neighbor embedding; TEA, triethyl amine; TFFH, tetramethylfluoriformamidinium hexafluorophosphate; VHL, von Hippel-Lindau

■ REFERENCES

- (1) Huang, H.; McGrath, A.; Audu, C. O.; Cernak, T. Catalyst: Systems Chemistry Links Reactions to Molecular Function. *Chem. 2024*, **10** (8), 2333–2336, DOI: 10.1016/j.chempr.2024.06.009.
- (2) Karageorgis, G.; Warriner, S.; Nelson, A. Efficient Discovery of Bioactive Scaffolds by Activity-Directed Synthesis. *Nat. Chem.* **2014**, **6** (10), 872–876.
- (3) Mahjour, B.; Shen, Y.; Liu, W.; Cernak, T. A Map of the Amine–Carboxylic Acid Coupling System. *Nature* **2020**, **580** (7801), 71–75.
- (4) Zhang, R.; Mahjour, B.; Outlaw, A.; McGrath, A.; Hopper, T.; Kelley, B.; Walters, W. P.; Cernak, T. Exploring the Combinatorial Explosion of Amine–Acid Reaction Space via Graph Editing. *Commun. Chem.* **2024**, **7** (1), 22.
- (5) Cyrus, K.; Wehenkel, M.; Choi, E.-Y.; Han, H.-J.; Lee, H.; Swanson, H.; Kim, K.-B. Impact of Linker Length on the Activity of PROTACs. *Mol. BioSyst.* **2011**, **7** (2), 359–364.
- (6) Bashore, F. M.; Foley, C. A.; Ong, H. W.; Rectenwald, J. M.; Hanley, R. P.; Norris-Drouin, J. L.; Cholensky, S. H.; Mills, C. A.; Pearce, K. H.; Herring, L. E.; Kireev, D.; Frye, S. V.; James, L. I. PROTAC Linkerology Leads to an Optimized Bivalent Chemical Degrader of Polycomb Repressive Complex 2 (PRC2) Components. *ACS Chem. Biol.* **2023**, **18** (3), 494–507.
- (7) Zoppi, V.; Hughes, S. J.; Maniaci, C.; Testa, A.; Gmaschitz, T.; Wieshofer, C.; Koegl, M.; Riching, K. M.; Daniels, D. L.; Spallarossa, A.; Ciulli, A. Iterative Design and Optimization of Initially Inactive Proteolysis Targeting Chimeras (PROTACs) Identify VZ185 as a Potent, Fast, and Selective von Hippel–Lindau (VHL) Based Dual Degrader Probe of BRD9 and BRD7. *J. Med. Chem.* **2019**, **62** (2), 699–726.
- (8) Hu, J.; Hu, B.; Wang, M.; Xu, F.; Miao, B.; Yang, C.-Y.; Wang, M.; Liu, Z.; Hayes, D. F.; Chinnaswamy, K.; Delproposto, J.; Stuckey, J.; Wang, S. Discovery of ERD-308 as a Highly Potent Proteolysis Targeting Chimera (PROTAC) Degrader of Estrogen Receptor (ER). *J. Med. Chem.* **2019**, **62** (3), 1420–1442.
- (9) Li, M.; Zhi, Y.; Liu, B.; Yao, Q. Advancing Strategies for Proteolysis-Targeting Chimera Design. *J. Med. Chem.* **2023**, **66** (4), 2308–2329.
- (10) Maple, H. J.; Clayden, N.; Baron, A.; Stacey, C.; Felix, R. Developing Degraders: Principles and Perspectives on Design and Chemical Space. *Med. Chem. Commun.* **2019**, **10** (10), 1755–1764.
- (11) Békés, M.; Langley, D. R.; Crews, C. M. PROTAC Targeted Protein Degraders: The Past Is Prologue. *Nat. Rev. Drug Discovery* **2022**, **21** (3), 181–200.
- (12) Papatzimas, J. W.; Evgeni, G.; Brownsey, Duncan K.; Maity, Ranjan.; Bahlis, Nizar J.; Derksen, Darren J. A General Strategy for the Preparation of Thalidomide-Conjugate Linkers. *Synlett* **2017**, **28** (20), 2881–2885.
- (13) Bhela, I. P.; Ranza, A.; Balestrero, F. C.; Serafini, M.; Aprile, S.; Di Martino, R. M. C.; Condorelli, F.; Pirali, T. A Versatile and Sustainable Multicomponent Platform for the Synthesis of Protein Degraders: Proof-of-Concept Application to BRD4-Degrading PROTACs. *J. Med. Chem.* **2022**, **65** (22), 15282–15299.
- (14) Klein, V. G.; Bond, A. G.; Craigon, C.; Lokey, R. S.; Ciulli, A. Amide-to-Ester Substitution as a Strategy for Optimizing PROTAC Permeability and Cellular Activity. *J. Med. Chem.* **2021**, **64** (24), 18082–18101.
- (15) Wurz, R. P.; Dellamaggiore, K.; Dou, H.; Javier, N.; Lo, M.-C.; McCarter, J. D.; Mohl, D.; Sastrí, C.; Lipford, J. R.; Cee, V. J. A “Click Chemistry Platform” for the Rapid Synthesis of Bispecific Molecules for Inducing Protein Degradation. *J. Med. Chem.* **2018**, **61** (2), 453–461.
- (16) Brownsey, D. K.; Rowley, B. C.; Gorobets, E.; Gelfand, B. S.; Derksen, D. J. Rapid Synthesis of Pomalidomide-Conjugates for the Development of Protein Degrader Libraries. *Chem. Sci.* **2021**, **12** (12), 4519–4525.
- (17) Hayhow, T. G.; Borrows, R. E. A.; Diène, C. R.; Fairley, G.; Fallan, C.; Fillery, S. M.; Scott, J. S.; Watson, D. W. A Buchwald–Hartwig Protocol to Enable Rapid Linker Exploration of Cereblon E3-Ligase PROTACs**. *Chem. - Eur. J.* **2020**, **26** (70), 16818–16823.
- (18) Guo, L.; Zhou, Y.; Nie, X.; Zhang, Z.; Zhang, Z.; Li, C.; Wang, T.; Tang, W. A Platform for the Rapid Synthesis of Proteolysis Targeting Chimeras (Rapid-TAC) under Miniaturized Conditions. *Eur. J. Med. Chem.* **2022**, **236**, No. 114317.
- (19) Qiu, X.; Sun, N.; Kong, Y.; Li, Y.; Yang, X.; Jiang, B. Chemoselective Synthesis of Lenalidomide-Based PROTAC Library Using Alkylation Reaction. *Org. Lett.* **2019**, **21** (10), 3838–3841.
- (20) Sosić, I.; Bricelj, A.; Steinebach, C. E3 Ligase Ligand Chemistries: From Building Blocks to Protein Degraders. *Chem. Soc. Rev.* **2022**, **51** (9), 3487–3534.
- (21) Boström, J.; Brown, D. G.; Young, R. J.; Keserü, G. M. Expanding the Medicinal Chemistry Synthetic Toolbox. *Nat. Rev. Drug Discovery* **2018**, **17** (10), 709–727.
- (22) Winter, G. E.; Buckley, D. L.; Paulk, J.; Roberts, J. M.; Souza, A.; Dhe-Paganon, S.; Bradner, J. E. Phthalimide Conjugation as a Strategy for in Vivo Target Protein Degradation. *Science* **2015**, **348** (6241), 1376–1381.
- (23) Mahjour, B.; Shen, Y.; Cernak, T. Ultrahigh-Throughput Experimentation for Information-Rich Chemical Synthesis. *Acc. Chem. Res.* **2021**, **54** (10), 2337–2346.
- (24) Shen, Y.; Borowski, J. E.; Hardy, M. A.; Sarpong, R.; Doyle, A. G.; Cernak, T. Automation and Computer-Assisted Planning for Chemical Synthesis. *Nat. Rev. Methods Primers* **2021**, **1** (1), 23.
- (25) Mahjour, B.; Zhang, R.; Shen, Y.; McGrath, A.; Zhao, R.; Mohamed, O. G.; Lin, Y.; Zhang, Z.; Douthwaite, J. L.; Tripathi, A.; Cernak, T. Rapid Planning and Analysis of High-Throughput Experiment Arrays for Reaction Discovery. *Nat. Commun.* **2023**, **14** (1), No. 3924.
- (26) Mahjour, B.; Hoffstadt, J.; Cernak, T. Designing Chemical Reaction Arrays Using Phactor and ChatGPT. *Org. Process Res. Dev.* **2023**, **27** (8), 1510–1516.
- (27) Wong, H.; Cernak, T. Reaction Miniaturization in Eco-Friendly Solvents. *Curr. Opin. Green Sustainable Chem.* **2018**, **11**, 91–98.
- (28) McGrath, A.; Zhang, R.; Shafiq, K.; Cernak, T. Repurposing Amine and Carboxylic Acid Building Blocks with an Automatable Esterification Reaction. *Chem. Commun.* **2023**, **59** (8), 1026–1029.
- (29) Shen, Y.; Mahjour, B.; Cernak, T. Development of Copper-Catalyzed Deaminative Esterification Using High-Throughput Experimentation. *Commun. Chem.* **2022**, **5** (1), 83.
- (30) Gruntz, U.; Katritzky, A. R.; Kenny, D. H.; Rezende, M. C.; Sheikh, H. Pyridines as Leaving Groups in Synthetic Transformations: Conversion of Amines into Esters. *J. Chem. Soc., Chem. Commun.* **1977**, No. 20, 701.

- (31) Ni, S.; Li, C.-X.; Mao, Y.; Han, J.; Wang, Y.; Yan, H.; Pan, Y. Ni-Catalyzed Deaminative Cross-Electrophile Coupling of Katritzky Salts with Halides via C–N Bond Activation. *Sci. Adv.* **2019**, *5* (6), eaaw9516.
- (32) Yi, J.; Badir, S. O.; Kammer, L. M.; Ribagorda, M.; Molander, G. A. Deaminative Reductive Arylation Enabled by Nickel/Photo-redox Dual Catalysis. *Org. Lett.* **2019**, *21* (9), 3346–3351.
- (33) Yue, H.; Zhu, C.; Shen, L.; Geng, Q.; Hock, K. J.; Yuan, T.; Cavallo, L.; Rueping, M. Nickel-Catalyzed C–N Bond Activation: Activated Primary Amines as Alkylating Reagents in Reductive Cross-Coupling. *Chem. Sci.* **2019**, *10* (16), 4430–4435.
- (34) Liao, J.; Basch, C. H.; Hoerrner, M. E.; Talley, M. R.; Boscoe, B. P.; Tucker, J. W.; Garnsey, M. R.; Watson, M. P. Deaminative Reductive Cross-Electrophile Couplings of Alkylpyridinium Salts and Aryl Bromides. *Org. Lett.* **2019**, *21* (8), 2941–2946.
- (35) Martin-Montero, R.; Yatham, V. R.; Yin, H.; Davies, J.; Martin, R. Ni-Catalyzed Reductive Deaminative Arylation at Sp₃ Carbon Centers. *Org. Lett.* **2019**, *21* (8), 2947–2951.
- (36) Wang, J.; Hoerrner, M. E.; Watson, M. P.; Weix, D. J. Nickel-Catalyzed Synthesis of Dialkyl Ketones from the Coupling of N-Alkyl Pyridinium Salts with Activated Carboxylic Acids. *Angew. Chem., Int. Ed.* **2020**, *59*, 13484.
- (37) Wang, J.; Ehehalt, L. E.; Huang, Z.; Beleh, O. M.; Guzei, I. A.; Weix, D. J. Formation of C(Sp₂)–C(Sp₃) Bonds Instead of Amide C–N Bonds from Carboxylic Acid and Amine Substrate Pools by Decarbonylative Cross-Electrophile Coupling. *J. Am. Chem. Soc.* **2023**, 1459951.
- (38) Amani, J.; Molander, G. A. Direct Conversion of Carboxylic Acids to Alkyl Ketones. *Org. Lett.* **2017**, *19* (13), 3612–3615.
- (39) Cornella, J.; Edwards, J. T.; Qin, T.; Kawamura, S.; Wang, J.; Pan, C.-M.; Gianatassio, R.; Schmidt, M.; Eastgate, M. D.; Baran, P. S. Practical Ni-Catalyzed Aryl–Alkyl Cross-Coupling of Secondary Redox-Active Esters. *J. Am. Chem. Soc.* **2016**, *138* (7), 2174–2177.
- (40) Prieto Kullmer, C. N.; Kautzky, J. A.; Krksa, S. W.; Nowak, T.; Dreher, S. D.; MacMillan, D. W. C. Accelerating Reaction Generality and Mechanistic Insight through Additive Mapping. *Science* **2022**, *376* (6592), 532–539.
- (41) Douthwaite, J. L.; Zhao, R.; Shim, E.; Mahjour, B.; Zimmerman, P. M.; Cernak, T. Formal Cross-Coupling of Amines and Carboxylic Acids to Form Sp₃–Sp₂ Carbon–Carbon Bonds. *J. Am. Chem. Soc.* **2023**, *145* (20), 10930–10937.
- (42) Malapit, C. A.; Bour, J. R.; Brigham, C. E.; Sanford, M. S. Base-Free Nickel-Catalysed Decarbonylative Suzuki–Miyaura Coupling of Acid Fluorides. *Nature* **2018**, *563* (7729), 100–104.
- (43) Fehér, P. P.; Stirling, A. Theoretical Study on the Formation of Ni(PR₃)(Aryl)F Complexes Observed in Ni-Catalyzed Decarbonylative C–C Coupling of Acyl Fluorides. *Organometallics* **2020**, *39* (14), 2774–2783.
- (44) Fu, M.-C.; Shang, R.; Cheng, W.-M.; Fu, Y. Boron-Catalyzed N-Alkylation of Amines Using Carboxylic Acids. *Angew. Chem., Int. Ed.* **2015**, *54* (31), 9042–9046.
- (45) Sorribes, I.; Junge, K.; Beller, M. Direct Catalytic N-Alkylation of Amines with Carboxylic Acids. *J. Am. Chem. Soc.* **2014**, *136* (40), 14314–14319.
- (46) Stoll, E. L.; Tongue, T.; Andrews, K. G.; Valette, D.; Hirst, D. J.; Denton, R. M. A Practical Catalytic Reductive Amination of Carboxylic Acids. *Chem. Sci.* **2020**, *11* (35), 9494–9500.
- (47) Zhang, Q.; Fu, M.-C.; Yu, H.-Z.; Fu, Y. Mechanism of Boron-Catalyzed N-Alkylation of Amines with Carboxylic Acids. *J. Org. Chem.* **2016**, *81* (15), 6235–6243.
- (48) Zengerle, M.; Chan, K.-H.; Ciulli, A. Selective Small Molecule Induced Degradation of the BET Bromodomain Protein BRD4. *ACS Chem. Biol.* **2015**, *10* (8), 1770–1777.
- (49) Jarusiewicz, J. A.; Yoshimura, S.; Mayasundari, A.; Actis, M.; Aggarwal, A.; McGowan, K.; Yang, L.; Li, Y.; Fu, X.; Mishra, V.; Heath, R.; Narina, S.; Pruett-Miller, S. M.; Nishiguchi, G.; Yang, J. J.; Rankovic, Z. Phenyl Dihydouracil: An Alternative Cereblon Binder for PROTAC Design. *ACS Med. Chem. Lett.* **2023**, *14* (2), 141–145.
- (50) Min, J.; Mayasundari, A.; Keramatinia, F.; Jonchere, B.; Yang, S. W.; Jarusiewicz, J.; Actis, M.; Das, S.; Young, B.; Slavish, J.; Yang, L.; Li, Y.; Fu, X.; Garrett, S. H.; Yun, M.-K.; Li, Z.; Nithianantham, S.; Chai, S.; Chen, T.; Shelat, A.; Lee, R. E.; Nishiguchi, G.; White, S. W.; Roussel, M. F.; Potts, P. R.; Fischer, M.; Rankovic, Z. Phenyl-Glutaramides: Alternative Cereblon Binders for the Design of PROTACs. *Angew. Chem., Int. Ed.* **2021**, *60* (51), 26663–26670.
- (51) Han, X.; Sun, Y. Strategies for the Discovery of Oral PROTAC Degraders Aimed at Cancer Therapy. *Cell Rep. Phys. Sci.* **2022**, *3* (10), No. 101062.
- (52) Riching, K. M.; Mahan, S.; Corona, C. R.; McDougall, M.; Vasta, J. D.; Robers, M. B.; Urh, M.; Daniels, D. L. Quantitative Live-Cell Kinetic Degradation and Mechanistic Profiling of PROTAC Mode of Action. *ACS Chem. Biol.* **2018**, *13* (9), 2758–2770.
- (53) Vasta, J. D.; Corona, C. R.; Robers, M. B. A High-Throughput Method to Prioritize PROTAC Intracellular Target Engagement/Target Engagement and Cell Permeability/Permeability Using Nano-BRET/NanoBRET. In *Targeted Protein Degradation: Methods and Protocols*; Cacace, A. M.; Hickey, C. M.; Békés, M., Eds.; Springer US: New York, NY, 2021; pp 265–282.
- (54) RBA Is Defined as the Ratio of a Compound’s Affinity in Live versus Permeabilized Cells. A Larger Right Shift in Measured Affinity in the Live-Cell Mode Leads to Larger RBA Values and Is an Indication of Lower Permeability.
- (55) Nowak, R. P.; DeAngelo, S. L.; Buckley, D.; He, Z.; Donovan, K. A.; An, J.; Safaei, N.; Jedrychowski, M. P.; Ponthier, C. M.; Ishoey, M.; Zhang, T.; Mancias, J. D.; Gray, N. S.; Bradner, J. E.; Fischer, E. S. Plasticity in Binding Confers Selectivity in Ligand-Induced Protein Degradation. *Nat. Chem. Biol.* **2018**, *14* (7), 706–714.
- (56) Schrödinger Release 2023–4.
- (57) Schrödinger Release 2023–4: Desmond Molecular Dynamics System.